

# Zinc Oxide Nanocomposites of Selected Polymers: Synthesis, Characterization, and Corrosion Inhibition Studies on Mild Steel in HCl Solution

Taiwo W. Quadri,<sup>†,‡</sup> Lukman O. Olasunkanmi,<sup>†,‡,§</sup> Omolola E. Fayemi,<sup>†,‡</sup> Moses M. Solomon,<sup>||</sup> and Eno E. Ebenso<sup>\*,†,‡,||</sup>

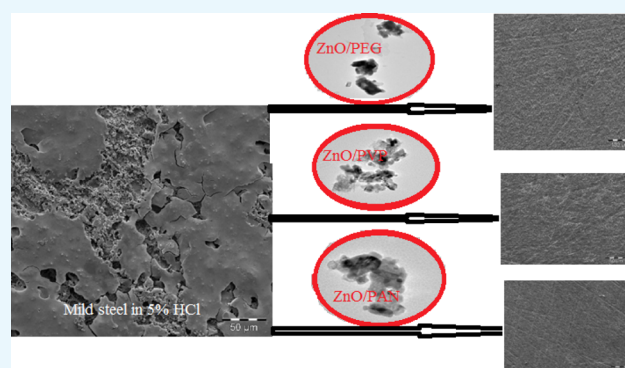
<sup>†</sup>Department of Chemistry, School of Mathematical and Physical Sciences, Faculty of Agriculture, Science and Technology and

<sup>‡</sup>Material Science Innovation and Modelling (MaSIM) Research Focus Area, Faculty of Agriculture, Science and Technology, North-West University (Mafikeng Campus), Private Bag X2046, Mmabatho 2735, South Africa

<sup>§</sup>Department of Chemistry, Faculty of Science, Obafemi Awolowo University, Ile-Ife 220005, Nigeria

<sup>||</sup>Department of Science Technology, Akwa-Ibom State Polytechnic, Ikot Osurua, P.M.B 2100, Ikot Ekpene, Nigeria

**ABSTRACT:** Nanocomposites of ZnO and some selected polymers, namely, poly(ethylene glycol), poly(vinylpyrrolidone), and polyacrylonitrile, were synthesized and characterized using Fourier transform infrared (FTIR) spectroscopy, ultraviolet–visible (UV–vis) spectroscopy, thermogravimetric analysis (TGA), and transmission electron microscopy (TEM) techniques. The FTIR and UV–vis spectra confirmed the successful formation of the polymer nanocomposites. TGA results revealed that the synthesized polymer nanocomposites are more thermally stable than the polymers alone. ZnO nanoparticles were about 50–75 nm in size, assumed a rodlike shape, and got embedded in the polymer matrices, as revealed by TEM images. Corrosion inhibition potentials of the synthesized ZnO/polymer nanocomposites were investigated for mild steel in 5% HCl solution using potentiodynamic polarization (PDP), linear polarization resistance, and electrochemical impedance spectroscopy measurements. The results showed that each ZnO/polymer nanocomposite inhibits mild steel corrosion in 5% HCl solution better than the respective polymer alone. The nanocomposites, according to PDP studies, behaved as a mixed-type inhibitor. The predominant mode of adsorption of the nanocomposites to a mild steel surface was found to be mixed type, and the adsorption process obeys the Langmuir adsorption isotherm model. Scanning electron microscopy images also revealed the protective attributes of the ZnO/polymer nanocomposites for mild steel in 5% HCl solution.



## 1. INTRODUCTION

Metals constitute a great part of materials in construction, medical, oil and gas, petrochemical, and allied industries. In these industries, the metallic material as a result of interaction with its surrounding environment loses its essential properties over a period of time. As a result, the material cannot perform the intended function effectively and reliably.<sup>1,2</sup> Corrosion of metals has numerous adverse consequences and has been long known to be a matter of serious concern to experts in both academia and industries.<sup>3</sup>

The use of inhibitor as a cost-effective and easiest method of repressing metal corrosion is a common fact. Organic compounds top the chart of metal corrosion inhibitors at present.<sup>4</sup> Nevertheless, some of these organic compounds are considered unfriendly to the ecosystem and expensive.<sup>5</sup> Polymers have been identified as potential ecofriendly and affordable corrosion inhibitors.<sup>6,7</sup> However, their limited solubility in common aqueous corrosive media and desorption at high temperatures have impeded their wide application as

corrosion inhibitors. Metal nanoparticles/polymer composites have proffered improvements over the earlier known limitations of polymers as corrosion inhibitors. Hefni et al.<sup>8</sup> reported that chitosan-grafted-poly(ethylene glycol) (Ch-g-mPEG) self-assembled on silver nanoparticles exhibited superior corrosion inhibiting ability (ca. 93%) for carbon steel in 1 M HCl solution compared to that of Ch-g-mPEG without silver nanoparticles (ca. 77%). The incorporation of silver nanoparticles into the matrix of poly(propylene glycol),<sup>9,10</sup> poly(methacrylic acid),<sup>11,12</sup> chitosan,<sup>13,14</sup> and carboxymethyl cellulose<sup>15</sup> had also been reported to enhance corrosion protection properties of the polymers.

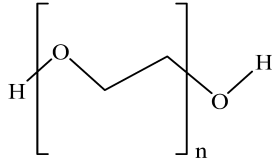
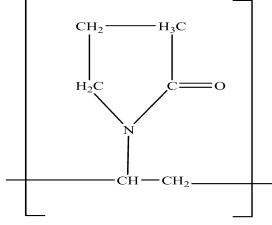
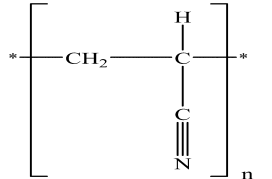
Metal oxide nanoparticles are of special interest due to their diverse mechanical, structural, thermal, electronic, magnetic, and optical properties. Among the wide variety of metal oxide nanoparticles, ZnO is one of the most promising because of its

Received: September 16, 2017

Accepted: October 31, 2017

Published: November 29, 2017

Table 1. Basic Information of Selected Polymers

Name of inhibitor	Molecular structure	Chemical formula	Molecular weight
Polyethylene glycol		$C_{2n}H_{4n+2}O_{n+1}$	3,350 g/mol
Polyvinylpyrrolidone		$(C_6H_9NO)_n$	10,000 g/mol
Polyacrylonitrile		$(C_3H_3N)_n$	150,000 g/mol

unique properties such as thermal and mechanical stability at room temperature, good physical and chemical stability, environmental friendliness, abundant availability, and low cost. There are reports on the utilization of polypyrrole/ZnO,<sup>16</sup> poly(*o*-phenylenediamine-*co*-aniline)/ZnO,<sup>17</sup> and polyaniline/ZnO<sup>18</sup> as anticorrosion additives in different corrosive environments. ZnO nanoparticles have also been found to improve the thermal behavior of polymers.<sup>19,20</sup>

To the best of our knowledge, corrosion inhibition potentials of nanocomposites of ZnO nanoparticles with poly(ethylene glycol) (PEG), poly(vinylpyrrolidone) (PVP), and polyacrylonitrile (PAN) have not been reported for mild steel in 5% HCl medium. This article therefore presents ZnO/PEG, ZnO/PVP, and ZnO/PAN nanocomposites as ecofriendly inhibitors of mild steel corrosion in 5% HCl solution. The synthesized ZnO/polymer nanocomposites were characterized using Fourier transform infrared (FTIR) spectroscopy, ultraviolet–visible (UV–vis) spectroscopy, thermogravimetric analysis (TGA), and transmission electron microscopy (TEM) techniques. Electrochemical methods such as potentiodynamic polarization (PDP), linear polarization resistance (LPR), and electrochemical impedance spectroscopy (EIS) techniques were used for corrosion rate measurements. Structural and molecular formulas as well as molecular weights of PEG, PVP, and PAN are given in Table 1.

## 2. MATERIALS AND METHODS

### 2.1. Mild Steel Composition and Surface Pretreatment.

The elemental compositions (in percentage by weight) of the mild steel used for corrosion studies are Fe (99.10), C (0.17), Mn (0.46), Si (0.26), S (0.017), and P (0.019). Encapsulation of the mild steel specimens in a Teflon holder with the aid of epoxy resin was done after cutting into 1 cm × 1 cm dimension, and the exposed surface area was 1 cm<sup>2</sup>. Struers MD Piano 220 fixed on a Struers LaboPol-1 machine was used for the mechanical abrasion of the metal coupons to get rid of remnants of epoxy resin and rust on the surface of the mild steel. Then, the polishing of the

mild steel specimens was done to near mirror image with emery papers of different grit sizes. Thereafter, the surface was washed under running water and degreased in acetone. All electrochemical experiments were conducted using mild steel coupons with a freshly pretreated surface.

**2.2. Chemicals.** Hydrochloric acid (32%) was commercially obtained from Promark Chemicals, South Africa, and diluted with distilled water to prepare 5% HCl solution, used as corrosion medium. Zn(NO<sub>3</sub>)<sub>2</sub>·6H<sub>2</sub>O and the polymers (PEG, PVP, and PAN) were purchased from Sigma-Aldrich Chemicals. Sodium hydroxide was purchased from Merck Chemicals.

**2.3. Synthesis.** **2.3.1. Synthesis of ZnO Nanoparticles.** Zinc nitrate, Zn(NO<sub>3</sub>)<sub>2</sub>·6H<sub>2</sub>O, was used as a precursor in preparing zinc oxide nanoparticles using chemical methods. NaOH pellets were dissolved in double-distilled water to prepare a 1.0 M concentration of the solution. The alkaline solution was heated up to 70 °C while being constantly stirred. After attaining 70 °C, 0.5 M Zn(NO<sub>3</sub>)<sub>2</sub>·6H<sub>2</sub>O was dripped for 1 h into the NaOH reaction flask while still stirring continuously. The system was kept at a steady temperature of 70 °C throughout the experiment. The resulting suspension formed from the slow addition of 0.5 M Zn(NO<sub>3</sub>)<sub>2</sub>·6H<sub>2</sub>O into the NaOH solution was allowed to stand at 70 °C for 2 h. Thereafter, the suspension was filtered, severally washed with double-distilled water, and then oven-dried at 65 °C for several hours.<sup>21</sup>

**2.3.2. Synthesis of ZnO/Polymer Nanocomposites.** ZnO/polymer (PEG, PVP, and PAN) nanocomposites were prepared by mixing aqueous solution of the respective polymer with the synthesized ZnO nanoparticles. First, different concentrations (100, 300, 500, 700, and 1000 ppm) of the respective polymers were prepared in 5% HCl solution. Then, respective concentrations of the polymer solution were used to prepare 1 mM ZnO nanoparticle solution. In the case of relatively insoluble PAN, it was initially dissolved in small quantity of dimethylformamide before mixing with ZnO nanoparticles.

**2.4. Characterization.** **2.4.1. FTIR Analysis.** Fourier transform infrared (FTIR) spectra of ZnO nanoparticles, PEG, PVP,

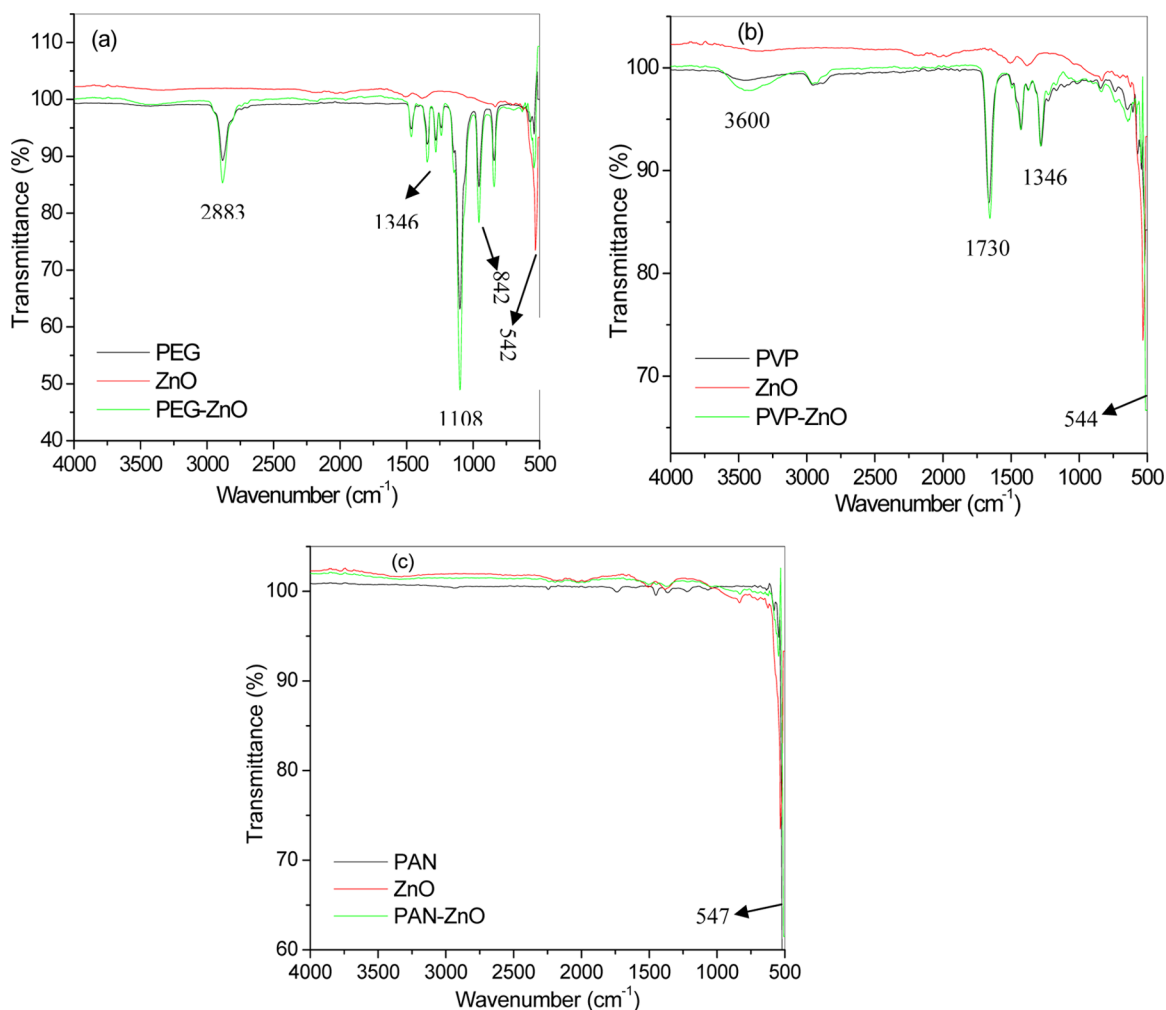


**Figure 1.** FTIR spectra of (a) PEG, ZnO, and ZnO/PEG (b) PVP, ZnO, and ZnO/PVP, and (c) PAN, ZnO, and ZnO/PAN.

PAN, and their respective ZnO/polymer nanocomposites were recorded using a Fourier transform infrared spectrophotometer (Agilent Technology, Cary 670 series FTIR spectrometer). The FTIR spectrum ranged from 4000 to 500  $\text{cm}^{-1}$ .

**2.4.2. UV–Visible Measurements.** UV–visible spectra analyses of the ZnO nanoparticles, PEG, PVP, PAN, and their respective ZnO/polymer nanocomposites were carried out using a UV–vis spectrophotometer (Agilent Technology, Cary 300 series UV–vis spectrometer) from 250 to 700 nm. Dual beam measurement mode was used at 1 nm resolution and 200 nm/min scan rate at 25  $^{\circ}\text{C}$ .

**2.4.3. TEM Analysis.** Transmission electron microscopy (TEM) measurements were used to determine the morphology and size of the synthesized ZnO nanoparticles and ZnO/polymer nanocomposites. A coat of ZnO nanoparticles and the ZnO/polymer nanocomposite sample on the copper grid was dried for 1 h. The TEM micrograph images were thereafter obtained and recorded using a JEOL JEM-2100F transmission electron microscope, Tokyo (Japan), operated at 200 kV.

**2.4.4. TGA Analysis.** Thermogravimetric analysis (TGA) was carried out on the ZnO nanoparticles, PEG, PVP, PAN, and their respective ZnO/polymer nanocomposites using an STA 1500 instrument. The TGA was conducted from 25 to 700  $^{\circ}\text{C}$  at a heating rate of 10  $^{\circ}\text{C min}^{-1}$  under nitrogen gas.

**2.5. Electrochemical Corrosion Studies.** Electrochemical corrosion measurements were performed on an Autolab

Potentiostat/Galvanostat 302 N instrument. The electrochemical system uses Ag/AgCl, 3 M KCl as the reference electrode and platinum rod as the counter electrode. A mild steel coupon serves as the working electrode. Before each measurement, the mild steel coupon was held in the corrosive medium for 30 min to attain a steady open circuit potential (OCP). Electrochemical measurements were performed after the attainment of a steady OCP. The impedance studies were conducted at the OCP by varying the frequency between 0.1 Hz and 100 kHz, and the impedance spectra were recorded at 10 mV amplitude. All electrochemical measurements were performed under aerated stagnant conditions at 303 K. The data generated was analyzed using Nova 1.10.1.9 software. From the value of the charge transfer parameter ( $R_{ct}$ ) derived from the analysis, the percentage inhibition efficiency ( $\eta$ ) of the inhibitor was calculated using eq 1

$$\eta_{\text{EIS}}(\%) = \frac{R_{ct} - R_{ct}^0}{R_{ct}} \quad (1)$$

where  $R_{ct}$  and  $R_{ct}^0$  are the charge transfer resistances in the presence and absence of inhibitors, respectively.

For potentiodynamic polarization studies, measurements were carried out at a constant scan rate of 1 mV/s by sweeping the potential in the range  $\pm 250$  mV with respect to the OCP. By extrapolating the linear sections of the polarization curves,

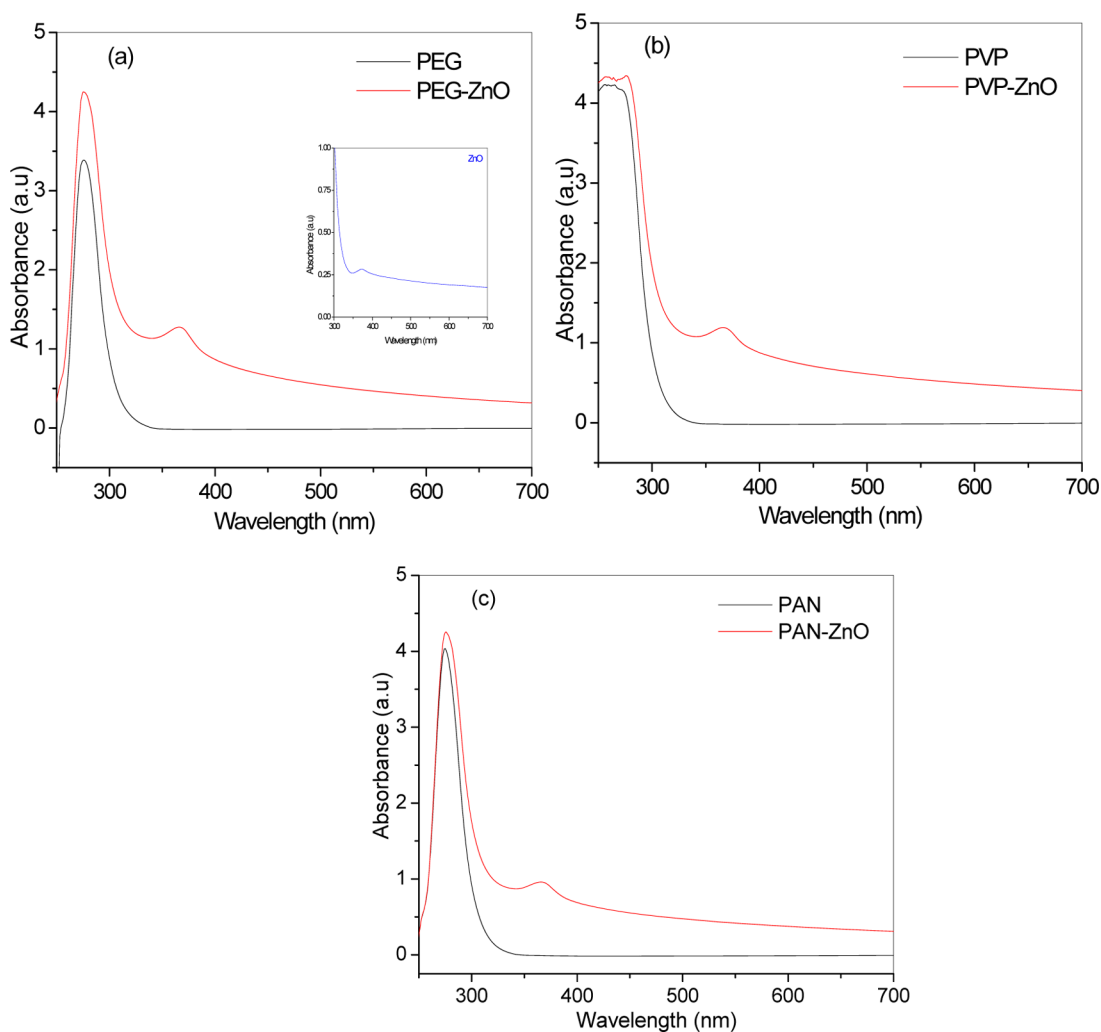


**Figure 2.** UV–visible spectra of (a) PEG and ZnO/PEG, (b) PVP and ZnO/PVP, and (c) PAN and ZnO/PAN. Inset (a): ZnO nanoparticles.

numerical values of the anodic Tafel slope ( $\beta_a$ ), cathodic Tafel slope ( $\beta_c$ ), corrosion potential ( $E_{\text{corr}}$ ), and corrosion current density ( $i_{\text{corr}}$ ) were obtained. The percentage inhibition efficiency,  $\eta$ , was calculated following eq 2

$$\eta_{\text{PDP}}(\%) = \frac{i_{\text{corr}}^0 - i_{\text{corr}}^i}{i_{\text{corr}}^0} \times 100 \quad (2)$$

where  $i_{\text{corr}}^i$  and  $i_{\text{corr}}^0$  are the corrosion current densities with and without the inhibitors, respectively.

For polarization resistance measurements, experiments were performed with a potential in the range  $\pm 250$  mV relative to OCP and the current response was studied at a scan rate of 0.125 mV/s. For the purpose of obtaining linear polarization resistance (LPR) graphs, the over-potential and current values were drawn on a linear scale. The slope of the graphs in the vicinity of the corrosion potential gave the polarization resistance ( $R_p$ ). The percentage inhibition efficiency from this technique was computed thus

$$\eta_{\text{LPR}} = \frac{R_p - R_p^0}{R_p} \times 100 \quad (3)$$

where  $R_p$  and  $R_p^0$  are the polarization resistance values with and without the inhibitors, respectively.

**2.6. Scanning Electron Microscopy (SEM) Analysis.** The surface morphologies of the mild steel specimens after immersion in 5% HCl without and with 1000 ppm of PEG, PVP, PAN, and their respective ZnO nanocomposites for 24 h were examined and recorded using a SEM JEOL JSM-6610 LV instrument.

### 3. RESULTS AND DISCUSSION

#### 3.1. Characterization of ZnO Nanoparticles and ZnO/Polymer Nanocomposite Formation.

**3.1.1. FTIR Studies.** Figure 1 represents the FTIR spectra of PEG, PVP, PAN, ZnO nanoparticles, and the nanocomposites of the respective polymers recorded at room temperature from 4000 to 500  $\text{cm}^{-1}$ . In the ZnO nanoparticle spectrum, the absorption band at 531  $\text{cm}^{-1}$  is typical of the Zn–O stretching vibration.<sup>22</sup> The presence of this distinct sharp peak in the ZnO spectrum confirms the formation of ZnO nanocrystals.<sup>23</sup> The FTIR spectra of PEG and ZnO/PEG nanocomposite in Figure 1a display similar bands. The sharp absorption peak at 2883  $\text{cm}^{-1}$  is due to the C–H stretching band and the peak noticed at 1346  $\text{cm}^{-1}$  corresponds to the C–O–H bending vibration. The observed peak at 842  $\text{cm}^{-1}$  corresponds to the long polymeric chain bending in the polymer, and the peak at 1108  $\text{cm}^{-1}$  is attributed to the C–O stretching vibration. However, by juxtaposing the spectrum of PEG to that of ZnO/PEG, it is noticed that the

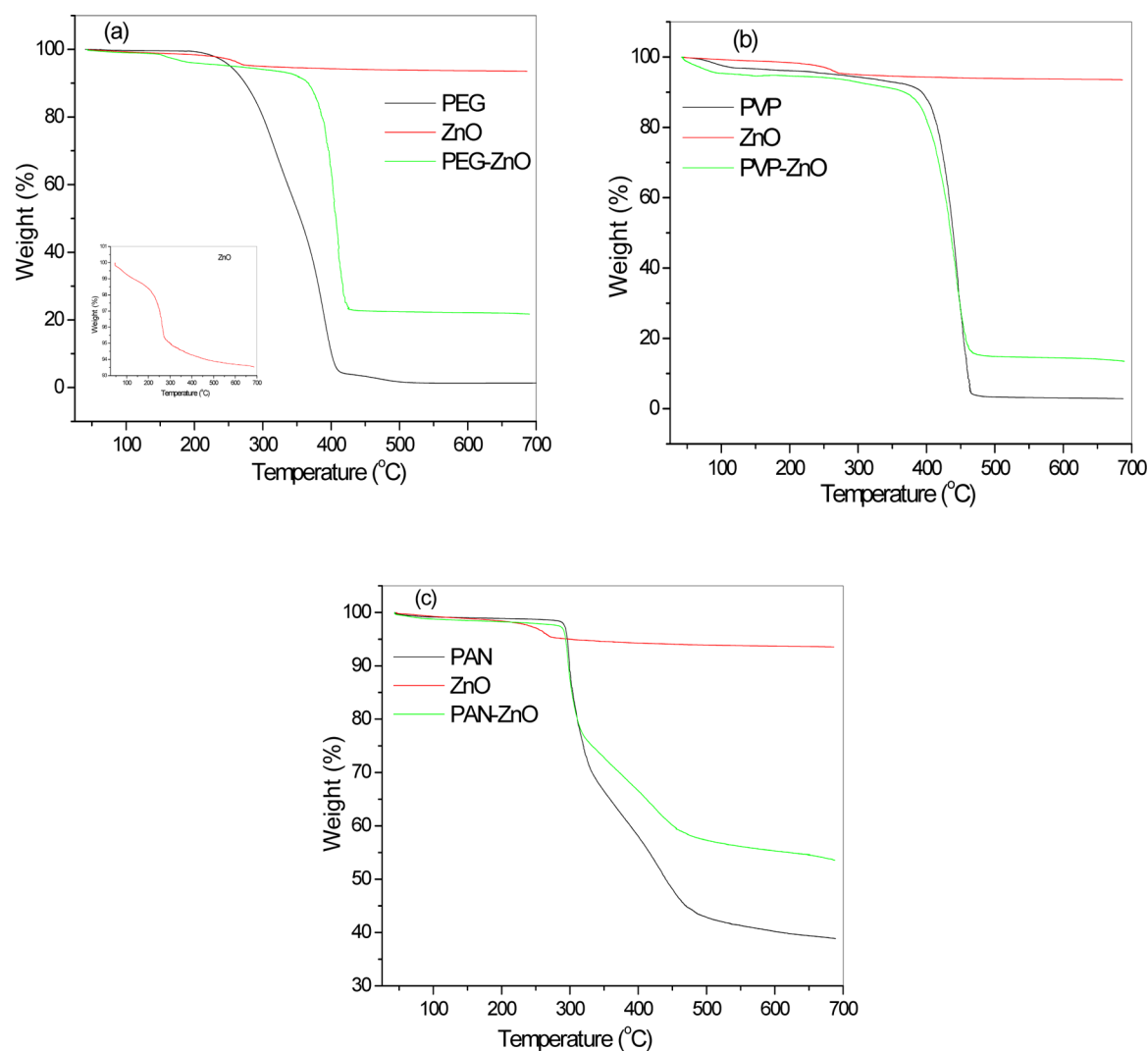


**Figure 3.** TGA curves of (a) PEG, ZnO, and ZnO/PEG, (b) PVP, ZnO, and ZnO/PVP, and (c) PAN, ZnO, and ZnO/PAN.

absorption bands at  $2883$  and  $1346\text{ cm}^{-1}$  are prominent in the ZnO/PEG spectrum. Again, it is observed that the Zn–O stretching mode at  $542\text{ cm}^{-1}$  in the ZnO spectrum is present in the ZnO/PEG nanocomposite spectrum. This suggests modification of PEG properties occasioned by the inclusion of ZnO nanoparticles. The broadness of the O–H stretching vibration peak at  $3600\text{ cm}^{-1}$  and the appearance of the Zn–O vibration mode at  $544\text{ cm}^{-1}$  in the ZnO/PVP spectrum relative to the PVP spectrum in Figure 1b may mean successful formation of ZnO/PVP. In Figure 1c, the Zn–O stretching band appears at  $547\text{ cm}^{-1}$ , also pointing to the formation of the ZnO/PAN nanocomposite.

**3.1.2. UV–Vis Studies.** The UV–vis absorption spectroscopy is a novel technique for the characterization of ZnO nanoparticles. The UV–vis spectrum of ZnO gives a characteristic peak at about  $360\text{--}380\text{ nm}$ .<sup>24–26</sup> Figure 2 shows the UV–vis absorption spectra for ZnO/PEG, ZnO/PVP, and ZnO/PAN nanocomposites, respectively. As could be seen in the figure, the ZnO characteristic peak is at  $368$ ,  $367$ , and  $372\text{ nm}$  in the ZnO/PEG, ZnO/PVP, and ZnO/PAN spectra, respectively, confirming the formation of the nanocomposites. The absorption band at about  $265\text{--}274\text{ nm}$  in the nanocomposite spectra is worth mentioning, which is caused by the  $\pi$  absorption of the functional groups in the polymers.<sup>27</sup>

**3.1.3. TGA Studies.** Thermogravimetric analysis is a reliable tool in determining the thermal behavior of substances, thermal degradation and weight loss, as it varies with temperature.<sup>28</sup> The TGA profiles of the synthesized ZnO nanoparticles, polymers, and polymer nanocomposites are shown in Figure 3. The TGA profile of ZnO nanoparticles reveals a total weight loss of  $6.10\%$  at about  $492\text{ }^{\circ}\text{C}$ , attributed to the removal of moisture content. No decomposition essentially occurs after this up to  $700\text{ }^{\circ}\text{C}$ , which is in perfect agreement with the report of Shamsuzzaman et al.<sup>25</sup> In Figure 3a, the TGA profile of ZnO/PEG shows an initial weight loss of  $4.19\%$  at about  $212\text{ }^{\circ}\text{C}$ , which is attributed to the elimination of water and volatile solvents. This is accompanied by a rapid weight loss of  $73.16\%$  at  $530\text{ }^{\circ}\text{C}$ . PEG was almost completely thermally decomposed at about  $420\text{ }^{\circ}\text{C}$ . At  $650\text{ }^{\circ}\text{C}$ , the residue of ZnO/PEG is about  $23\%$ , whereas that of PEG is less than  $1.00\%$ . This confirms that the presence of ZnO nanoparticles in the polymer nanocomposite improves its thermal stability.<sup>29</sup>

ZnO/PVP demonstrates three stages of weight loss, as seen in Figure 3b. At the first stage, there is  $8.13\%$  weight loss from  $25$  to  $308\text{ }^{\circ}\text{C}$ , which is attributed to the removal of residual solvent present in the nanocomposite. The second stage has a weight loss of  $76.80\%$ , which started at  $308\text{ }^{\circ}\text{C}$  and ended at about  $502\text{ }^{\circ}\text{C}$  due to the decomposition of PVP chains. Finally, an insignificant

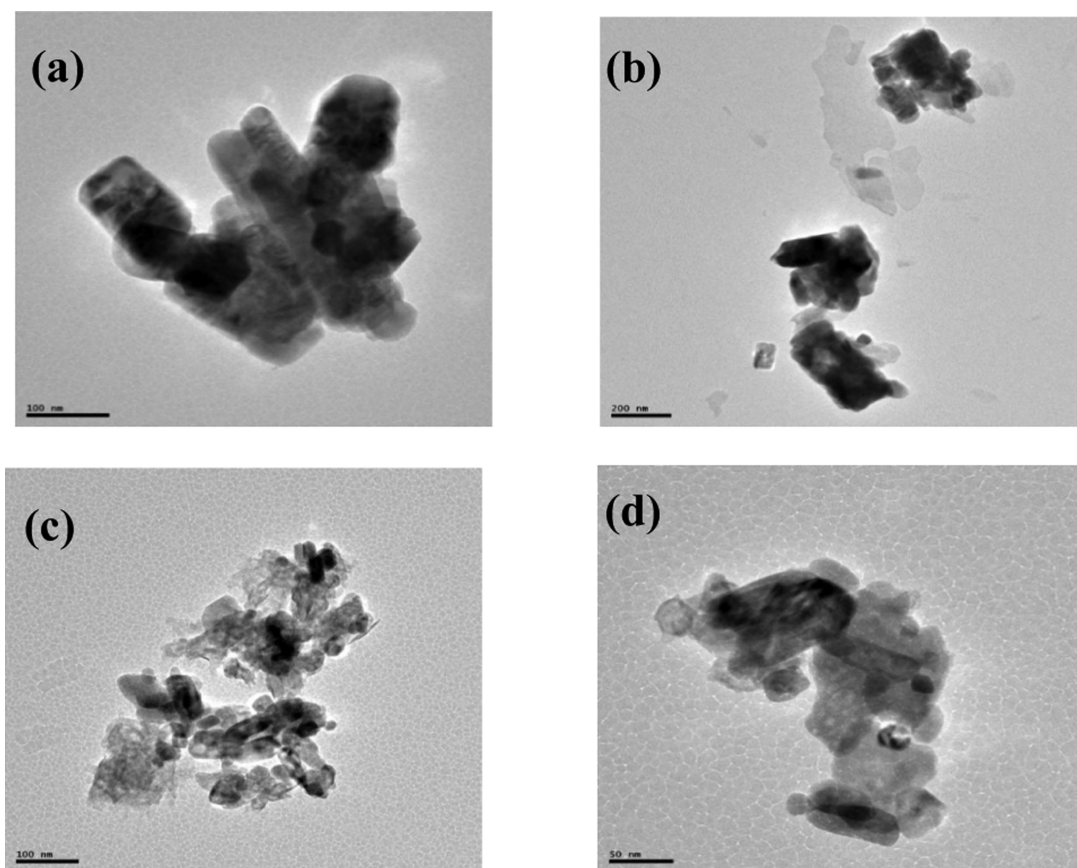


**Figure 4.** TEM images of (a) ZnO nanoparticles, (b) ZnO/PEG, (c) ZnO/PVP, and (d) ZnO/PAN nanocomposites.

loss of about 1.00% occurred at 641 °C, and it is expected that the only change at this stage is in the crystal structure. It is observed that PVP is completely decomposed at 641 °C leaving only the carbon residue. From the thermal behavior of PVP observed in the curve, it is seen that an initial weight loss of 4.71% occurred at 270 °C, followed by a significant weight loss of 90.38% between 270 and 464 °C, which represents the decomposition of the polymer. The ZnO/PVP nanocomposite is more thermally stable compared with PVP, and this can be attributed to the higher chain compactness due to the interaction between the PVP and ZnO nanoparticles.<sup>30</sup>

For PAN shown in Figure 3c, 1.40% weight loss is observed at 268 °C due to the loss of moisture, low molecular weight oligopolymers, and dehydrogenation. This is followed by a rapid weight loss of 32.00% within the temperature range of 267 and 350 °C. In the last stage, 23.08% weight loss occurs at about 485 °C, leading to reduction in the weight of PAN. The ZnO/PAN nanocomposite has weight losses of 2.24% at 267 °C at the first stage, 21.81% at 324 °C at the second stage, and 18.17% at 485 °C at the third stage. It is observed that whereas the total weight loss of 56.48% is recorded for PAN at about 485 °C, the nanocomposite containing ZnO nanoparticles has a weight reduction of 42.22% at the same temperature and a higher residue. These results again agree with the aforementioned that the presence of the ZnO nanoparticles in the polymer backbone reduces weight loss and promotes the formation of a thermally stable structure due to ionic and molecular cross-linking.<sup>31,32</sup> The observed improvement in the thermal stability of the polymers upon embedment of ZnO nanoparticles suggests that ZnO/polymer nanocomposites promise to perform better and last longer than the ordinary polymer when used for high-

temperature industrial processes where corrosion needs to be inhibited.

**3.1.4. TEM Studies.** The surface morphologies of the ZnO nanoparticles and polymer nanocomposites observed using TEM are shown in Figure 4. The TEM image of the ZnO nanoparticles as presented in Figure 4a reveals that the ZnO nanoparticles are crystalline and rodlike. Matinise et al.<sup>24</sup> had recently reported that ZnO nanoparticles synthesized using *Moringa oleifera* extract as the chelating agent appear rodlike. The sizes of the synthesized ZnO nanoparticles are in the range of 50–75 nm. The presence of aggregated ZnO nanoparticles is evident from the TEM image. It is obvious from Figure 4b–d that the ZnO nanoparticles are embedded inside the matrix of the respective polymer. The images again confirm the successful synthesis of ZnO nanoparticles and ZnO/polymer nanocomposites.

### 3.2. Electrochemical Corrosion Assessments.

**3.2.1. OCP–Time Profile, PDP, and LPR Studies.** OCP–time profiles for mild steel in 5% HCl in the presence of various concentrations of the polymer/ZnO nanocomposites are shown in Figure 5. The profiles revealed that the systems attained a stable OCP before the first 600 s after immersion in the corrosive media. Therefore, the adopted 30 min waiting period before electrochemical disturbance can be adjudged sufficient for OCP stabilization. More so, there is a marked difference between the equilibrium OCP values of the blank and inhibited systems. This suggests that the polymer/ZnO nanocomposites have some influence on the electrochemical (corrosion) process occurring in the aggressive solution. The OCP values in the presence of PEG/ZnO (at various concentrations) are generally more anodic than those of the blank, indicating that the steel is nobler in the

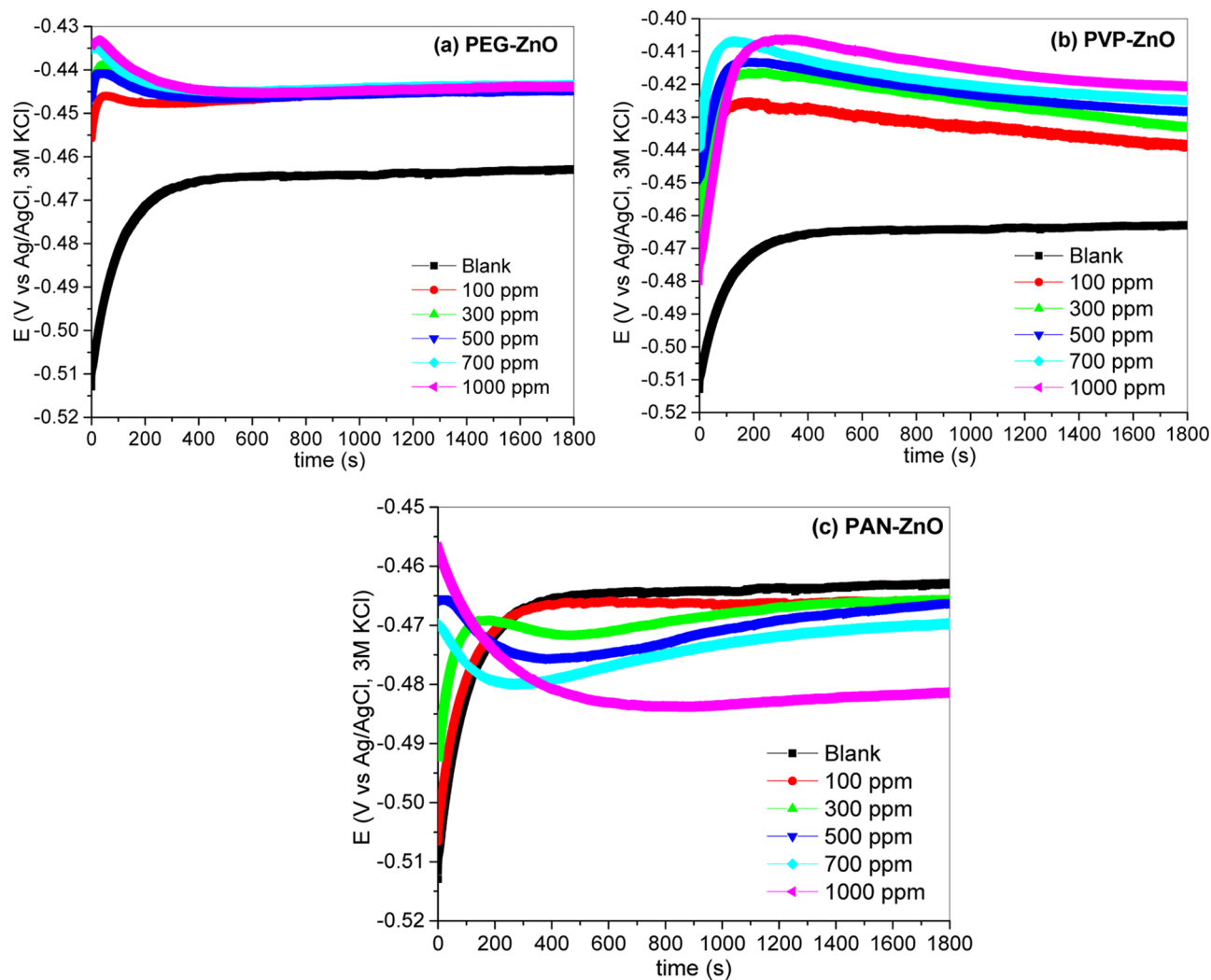


**Figure 5.** Variation of OCP with time for mild steel in 5% HCl without and with different concentrations of polymer/ZnO nanocomposites.

presence of PEG/ZnO compared with 5% HCl (with the additive). Similar observations were recorded in the presence of PVP/ZnO. On the other hand, the OCP values in the presence of PAN/ZnO are more cathodic than those of the blank. These observations suggest that PEG/ZnO and PVP/ZnO might have more influence on anodic mild steel oxidation in 5% HCl than on the accompanying cathodic reduction reaction, whereas PAN/ZnO might preferentially affect the cathodic reaction more than the anodic half-reaction.

The polarization curves derived from potentiodynamic polarization experiments on the working electrode in 5% HCl devoid of and containing various concentrations of ZnO/PEG, ZnO/PVP, and ZnO/PAN respectively at 303 K are presented in Figure 6. The associated polarization parameters are presented in Table 2. The figure reveals that the introduction of the studied inhibitors into the acidic medium reduced current densities at the anodic and cathodic sites. The inhibitors slightly shifted the corrosion potential to a noble position except ZnO/PAN that displaced the corrosion potential cathodically. This observation suggests that although the nanocomposites exhibit mixed-type tendency the ZnO/PEG and ZnO/PVP retard the dissolution of the mild steel at the anode better than the reduction of hydrogen ion at the cathode, whereas ZnO/PAN principally affects the cathodic reactions.<sup>9</sup> The addition of polymers and ZnO/polymer nanocomposites to the corrosive medium caused a decrease in

$i_{\text{corr}}$  value compared to the value for the blank system, as seen in Table 2. This result is seen to be determined by the quantity of the studied inhibitor used, and the direct effect is an increment in the inhibition performance of the nanocomposite. At 1000 ppm, ZnO/PAN affords 83.42% protection efficiency, whereas the same concentration for ZnO/PVP and ZnO/PEG offers 74.50 and 69.43%, respectively. The values of both  $\beta_a$  and  $\beta_c$  for inhibitor-containing systems were compared to those of the blank, and only a little change was observed. This suggests that ZnO/PEG, ZnO/PVP, and ZnO/PAN adsorb on the metal surface in 5% HCl solution by the geometric blocking mechanism.<sup>9</sup>

The values of  $R_p$  and the calculated  $\eta_{\text{LPR}}$  obtained from LPR measurements are also listed in Table 2. The results show that the  $R_p$  values for various concentrations of the studied inhibitors are greater than those of the blank solution. This again reflects the effectiveness of the polymer nanocomposites in boosting the corrosion resistance of the studied metal in 5% HCl solution. There is good agreement between the  $\eta_{\text{LPR}}$  and  $\eta_{\text{PDP}}$  values.

**3.2.2. EIS Studies.** The impedance of an electrochemical system over a frequency range can be measured using electrochemical impedance spectroscopy (EIS). The frequency response of a mild steel working electrode in relation to electrochemical reactions occurring at the electrode/electrolyte interface can be described by EIS measurements. Nyquist, Bode

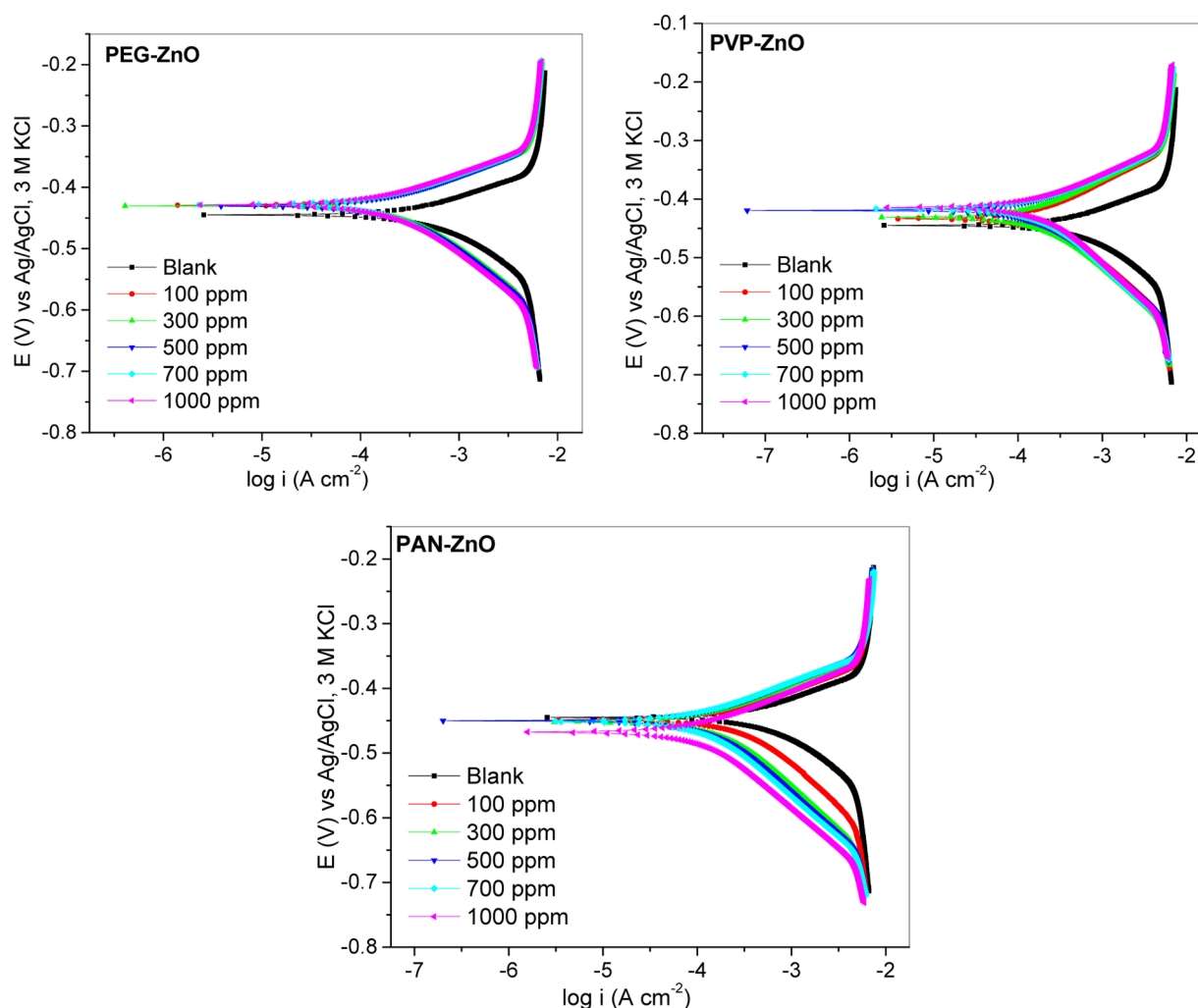


**Figure 6.** Potentiodynamic polarization plots for mild steel in 5% HCl in the absence and presence of different concentrations of (a) ZnO/PEG, (b) ZnO/PVP, and (c) ZnO/PAN.

**Table 2. Parameters Obtained from the Potentiodynamic and Linear Polarization of Mild Steel in 5% HCl in the Presence and Absence of Different Concentrations of Additives**

inhibitor	inhibitor conc. (ppm)	PDP					LPR	
		$-E_{\text{corr}}$ (mV)	$i_{\text{corr}}$ ( $\mu\text{A}/\text{cm}^2$ )	$\beta_a$ (mV/dec)	$\beta_c$ (mV/dec)	$\eta_{\text{PDP}}$ (%)	$R_p$ ( $\Omega \text{ cm}^2$ )	$\eta_{\text{LPR}}$ (%)
blank	0	445.05	655.25	118.95	89.77		33.91	
ZnO/PEG	100	419.35	244.23	114.12	74.27	62.73	80.00	57.61
	300	430.27	231.90	103.72	72.88	64.61	80.16	57.70
	500	430.42	210.28	103.93	67.93	67.91	84.84	60.00
	700	428.41	208.50	116.17	67.17	68.18	88.65	61.75
	1000	428.53	200.31	115.31	69.95	69.43	94.40	64.08
ZnO/PVP	100	433.27	205.52	106.23	86.12	68.64	100.50	66.26
	300	430.95	204.38	125.80	83.94	68.81	106.98	68.30
	500	419.66	184.11	125.83	74.31	71.90	110.20	69.23
	700	416.66	176.04	130.37	71.04	73.13	113.34	70.08
	1000	414.12	167.06	115.40	71.27	74.50	114.53	70.39
ZnO/PAN	100	448.34	380.28	149.65	76.92	41.96	57.95	41.48
	300	451.73	237.96	150.34	78.14	63.68	93.83	63.86
	500	450.16	191.61	146.24	73.70	70.76	111.07	69.47
	700	451.09	138.19	133.30	64.77	78.91	137.00	75.25
	1000	467.79	108.67	123.13	64.30	83.42	168.82	79.91

phase angle, and Bode modulus diagrams can be used to represent electrochemical impedance spectra. However, some scholars have recommended Bode modulus as the easiest and

most appropriate of the three popular impedance diagrams because the dispersion of the experimental data is minimized and it gives a better insight into the frequency-dependent response of



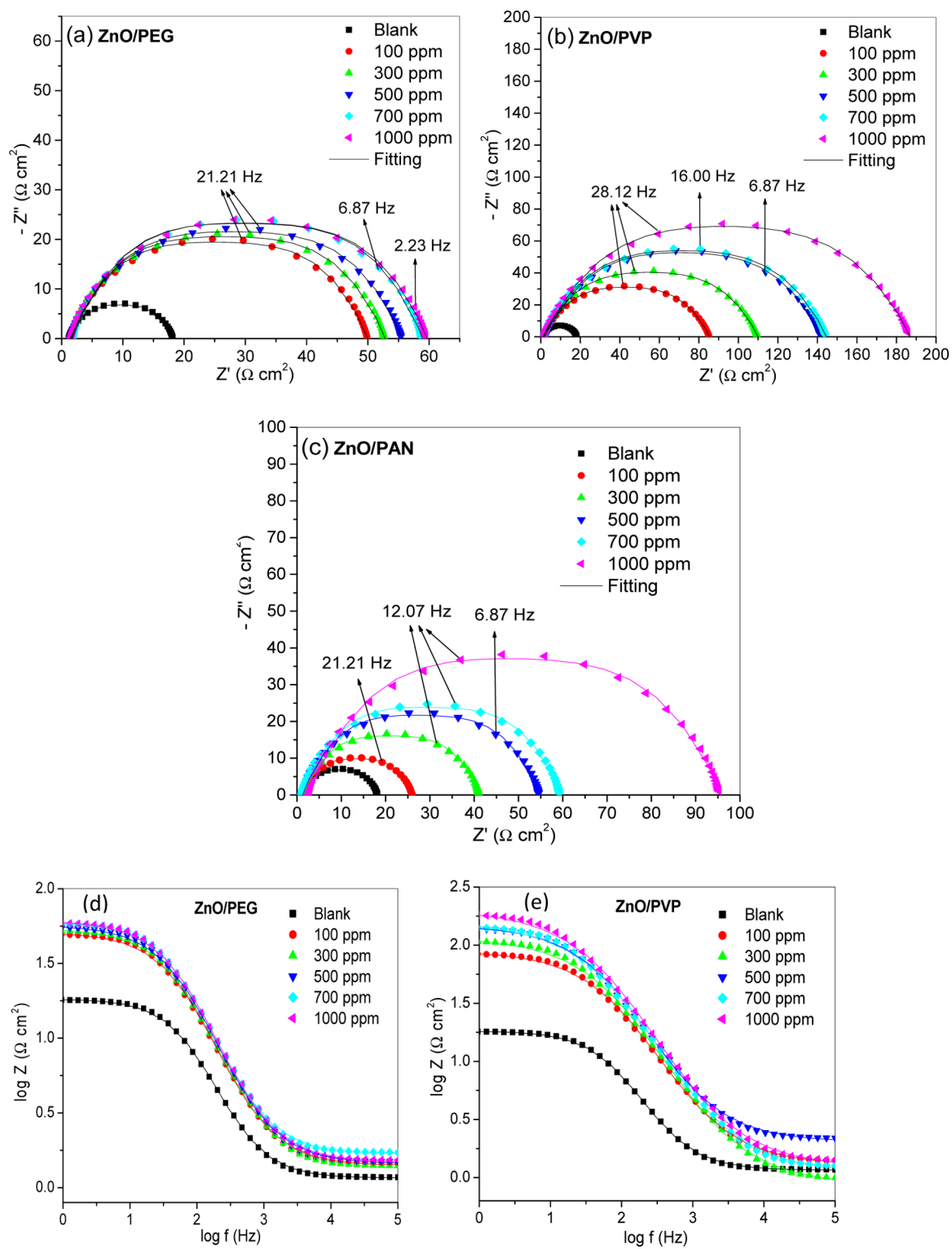
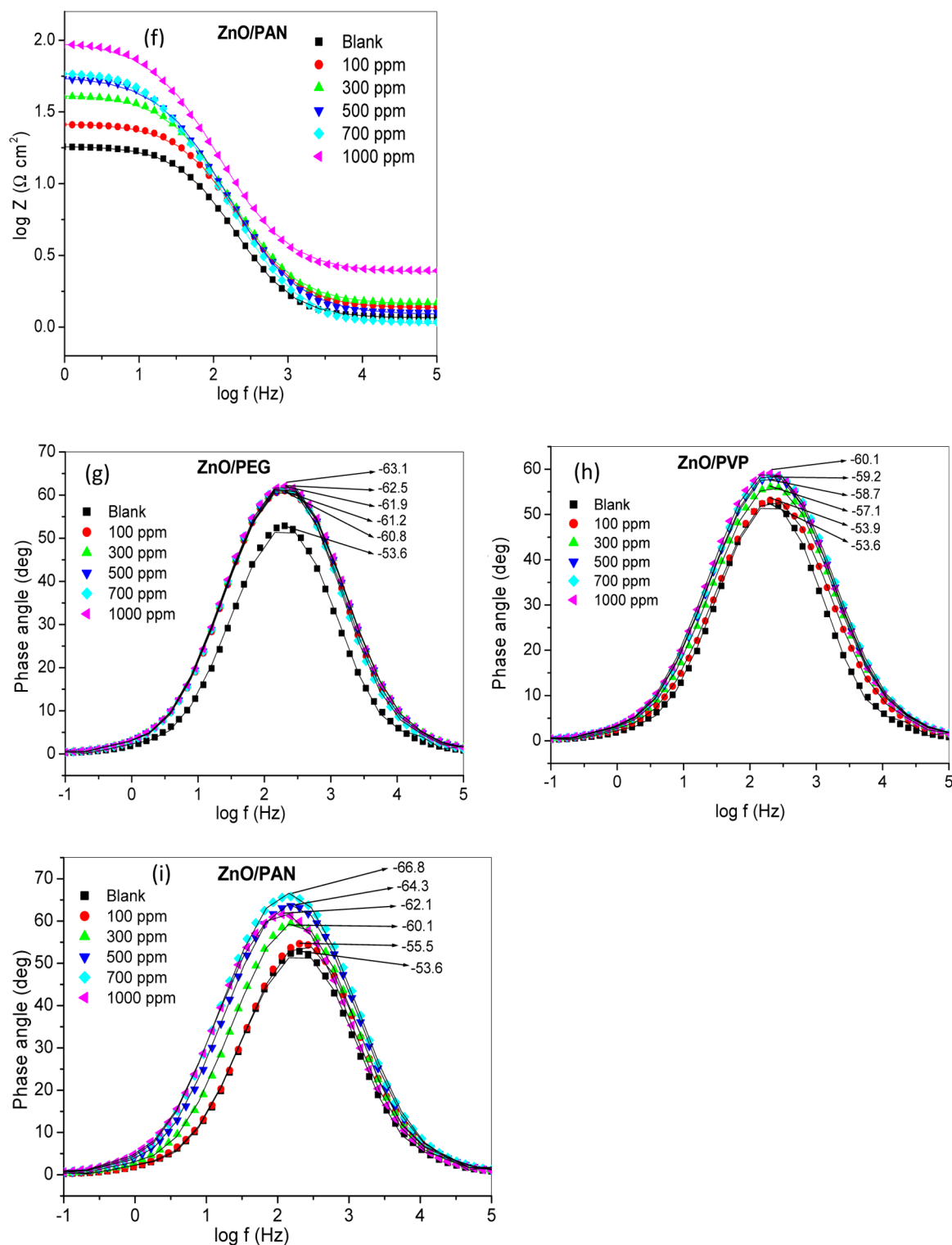


Figure 7. continued



**Figure 7.** Nyquist (a–c), Bode (d–f), and phase angle (g–i) plots for mild steel in 5% HCl without and with different concentrations of ZnO/polymer nanocomposites

the system. However, many authors choose to exploit the three representations in their studies,<sup>33,34</sup> as each plot provides some unique information about the interfacial phenomena that take place in the system. The EIS spectra for mild steel in 5% HCl for the blank and inhibitor-containing media at 303 K are presented in Figure 7. The impedance diagrams in Figure 7a–c contain depressed and imperfect semicircles, which are the characteristic features of solid working electrodes, indicating frequency

dispersions of interfacial impedance.<sup>35</sup> This feature is ascribed to fracture structures, distribution of activity centers, coarseness of the working electrode surface, adsorption of inhibitors, and formation of porous layers.<sup>13,36</sup> The single depressed semicircles in the Nyquist plots are analogous to a single time constant in the Bode diagrams in Figure 7d–f. This suggests that the corrosion of the mild steel is mainly dominated by a single charge transfer process.<sup>13,14,36</sup> A comparison of the impedance spectra recorded

in the corrosive solution devoid of inhibitor to those recorded in acid solution enriched with inhibitor reveals some similarity in the profiles. This indicates that the studied inhibitors did not alter the corrosion mechanism of the metal specimen in the corrosive environment.<sup>37,38</sup> However, the impedance spectra of the inhibited systems are larger in size than those of the uninhibited system. The Bode diagrams exhibited increased area under the phase angle curves with the addition of the studied inhibitors compared to that for the uninhibited solution.<sup>39</sup> The observed increment is clearly a function of inhibitor concentration, which suggests that more inhibitor molecules adsorb on the mild steel surface and a protective film is formed. An increase in the amount of the inhibitor may have led to a greater surface coverage. This is also obvious in the Bode modulus (Figure 7d–f) and phase angle (Figure 7g–i) plots, i.e., an increase in the concentration of nanocomposites increases the impedance modulus at low frequencies as well as the phase angles.

Figure 8 presents the electrical equivalent circuit used for analyzing the impedance spectra. Simulation results for ZnO/

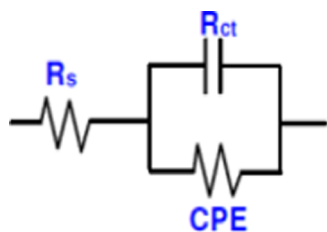


Figure 8. Randle's equivalent circuit.

polymer nanocomposites show that this electrical equivalent circuit accurately fits to the experimental data (Figure 9 and Table 3). Randle's equivalent circuit comprises a resistor of solution resistance ( $R_s$ ) and a resistor of charge transfer resistance ( $R_{ct}$ ), which are in parallel connection with the constant phase element (CPE). CPE was introduced in the equivalent circuit instead of a pure double-layer capacitor ( $C_{dl}$ ) to get a more accurate fit. However, the  $C_{dl}$  values were computed from the  $Y_0$  and  $n$  values, which are the magnitudes of CPE and deviation parameter ( $-1 \leq n \leq 1$ , which is dependent on surface morphology) using eq 4.<sup>40,41</sup> The inhibition efficiency was computed using eq 1. The estimated electrochemical parameters are listed in Table 3.

$$C_{dl} = (Y_0 R_{ct}^{1-n})^{1/n} \quad (4)$$

The results (in Table 3) show that  $R_{ct}$  values in the presence of inhibitors are greater than those of uninhibited medium and increase with an increase in inhibitor concentration. As the  $R_{ct}$  value increases, the inhibition efficiency increases. Again, this emphasizes the dependency of inhibition performance on the concentration of the inhibitor. The  $n$  values are close to unity, suggesting the pseudocapacitive characteristics of the electrode/electrolyte interface.<sup>42,43</sup> It is also clear from the table that the  $C_{dl}$  value declines steadily with an increasing amount of inhibitor. This decline in the value of  $C_{dl}$  can be interpreted using the Helmholtz equation

$$C_{dl} = \frac{\epsilon \epsilon_0}{d} \quad (5)$$

where  $\epsilon$  represents the dielectric constant of the protective layer,  $\epsilon_0$  represents the permittivity of free space, and  $d$  is the thickness of the double layer. This implies that an increase in  $d$  or a

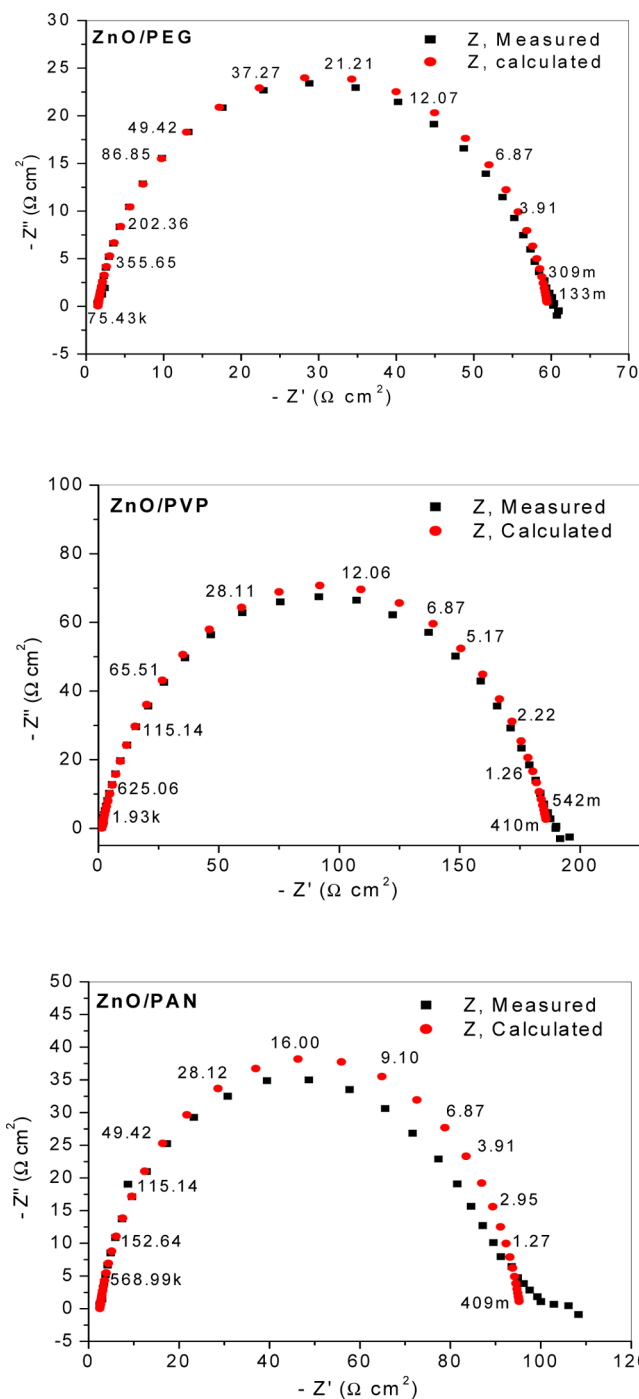


Figure 9. Simulation impedance diagrams for ZnO/polymer nanocomposites.

decrease in  $\epsilon$  can cause a decrease in the value of  $C_{dl}$ . Therefore, the decrease in  $C_{dl}$  value with an increasing inhibitor concentration in the present investigation is due to greater surface coverage as the inhibitor concentration was increased, which agrees with the behavior of  $\eta$  with increasing inhibitor concentration.

A quick comparison of the inhibition efficiency of ZnO/polymer nanocomposites of the present work with those reported in the literature (Table 4) reveals that although the inhibition efficiency is not the same, it compares well. Factors such as differences in the concentration of the corrosive medium, chemical composition of the polymer, and the concentration of ZnO/polymer used might

**Table 3. EIS Parameters for Mild Steel in 5% HCl in the Absence and Presence of Different Concentrations of ZnO/PEG, ZnO/PVP, and ZnO/PAN**

inhibitor	concentration (ppm)	$R_s$ ( $\Omega$ cm <sup>2</sup> )	$R_{ct}$ ( $\Omega$ cm <sup>2</sup> )	$n$	$Y_0$ ( $\mu\Omega$ s <sup><math>n</math></sup> cm <sup>-2</sup> )	$C_{dl}$ ( $\mu$ F cm <sup>-2</sup> )	$\chi^2$	$\eta_{EIS}$ (%)
blank	0	1.17	17.0	0.886	425	225.31	0.93782	
ZnO/PEG	100	1.44	48.5	0.882	226	123.54	0.83012	64.95
	300	1.39	51.3	0.880	221	119.94	0.84808	66.86
	500	1.49	54.0	0.879	211	113.93	0.81760	68.52
	700	1.72	57.0	0.892	186	107.24	0.87970	70.18
	1000	1.52	58.0	0.882	197	108.29	0.80383	70.69
ZnO/PVP	100	1.37	83.9	0.826	171	69.91	1.52870	79.74
	300	0.97	109.0	0.828	154	65.90	1.08390	84.40
	500	2.16	139.0	0.839	126	57.98	1.42690	87.77
	700	1.24	143.0	0.839	127	57.52	0.92192	88.11
	1000	1.38	185.0	0.831	120	55.31	1.06700	90.81
ZnO/PAN	100	1.38	24.6	0.879	308	157.22	0.84234	30.89
	300	1.47	39.6	0.888	271	152.99	1.36560	57.07
	500	1.26	53.3	0.891	270	160.75	1.45950	68.11
	700	1.08	58.2	0.897	284	177.34	1.11630	70.79
	1000	2.47	93.0	0.877	202	143.25	1.49320	81.72
PEG	1000	1.78	56.1	0.882	210	115.91	0.99105	69.70
PVP	1000	4.13	142.0	0.857	93	45.16	1.06360	88.03
PAN	1000	2.23	85.4	0.883	218	128.60	1.52310	80.09

**Table 4. Comparison of the Percentage Inhibition Efficiency of ZnO/Polymer Nanocomposites for Steel Obtained in the Present Study with Some Literature Values**

S/N	ZnO/polymer nanocomposite	medium	% $\eta$	ref
1	ZnO/polyacrylamide nanocomposite	1 M HCl	90.09	60
2	ZnO/poly(aniline-co-2-pyridylamine-co.2,3-xylidine)	0.1 M HCl	97.27	45
3	ZnO/chitosan	0.1 N HCl	73.80	53
4	ZnO/PEG	5% HCl	70.69	present work
5	ZnO/PVP		90.81	
6	ZnO/PAN		81.72	

be responsible for the observed variation in inhibition efficiency. It could be concluded from Table 4 that the ZnO/polymer nanocomposite is effective in inhibiting steel corrosion in HCl environment. Umoren and Solomon<sup>44</sup> had classified corrosion inhibitors with percentage inhibition efficiency greater than 70% as excellent inhibitors.

**3.3. Effect of ZnO Nanoparticles on the Inhibition Efficiency of the Polymers.** To examine the effect of the ZnO nanoparticles on the inhibitive ability of the polymers in the acid solution, EIS experiments were undertaken with 1000 ppm polymers and their respective ZnO/polymer nanocomposites. The comparative Nyquist plots are shown in Figure 10. As could be seen in the figure, the diameter of the respective nanocomposite capacitive loop is bigger than that of the corresponding polymer. This clearly shows an improved inhibition performance of the studied polymers, which can be attributed to the presence of ZnO nanoparticles. It is noticed from Table 3 that the presence of ZnO nanoparticles raised the  $R_{ct}$  value for PEG, PVP, and PAN from 56.1, 142.0, and 85.4  $\Omega$  cm<sup>2</sup>, respectively, to 58.0, 185.0, and 93.0  $\Omega$  cm<sup>2</sup>. The inhibition efficiency is stepped up from 69.70, 88.03, and 80.09% for PEG, PVP, and PAN, respectively, to 70.69, 90.81, and 81.72% for the respective ZnO/polymer nanocomposites. This seems to suggest that the ZnO nanoparticles induce the participation of more of the polymer active sites in the adsorption process or they interact directly with the metal surface. According to Solomon et al.,<sup>14,15</sup> metal nanoparticles have the tendency to directly chemisorb on a mild steel surface.

**3.4. Adsorption Consideration.** An adsorption isotherm model was deployed to ascertain the mode of adsorption of the studied ZnO/polymer nanocomposites onto a mild steel surface in 5% HCl medium. The experimental data were tested with diverse isotherm models, including Freundlich, Temkin, El-Awady et al., and Langmuir adsorption isotherm. By virtue of the linear regression values ( $R^2$ ) in Figure 11, the best line of fit for the adsorption process was obtained with the Langmuir adsorption isotherm model. The Langmuir isotherm model is expressed as<sup>45</sup>

$$\frac{C_{inh}}{\theta} = \frac{1}{K_{ads}} + C_{inh} \quad (6)$$

where  $\theta$  represents the surface coverage,  $K_{ads}$  represents the adsorption equilibrium constant, and  $C_{inh}$  represents the concentration of the inhibitors. The graphs of  $C_{inh}/\theta$  against  $C_{inh}$  for the studied systems are presented in Figure 11. Obviously, the graphs are all linear and the  $R^2$  values are near unity, suggesting that the adsorption of ZnO/polymer nanocomposites onto the steel surface in 5% HCl solution is best described by this model. However, a close look at the figure reveals that the slope deviated slightly from unity, required by the ideal Langmuir isotherm model. This is not surprising as the possibility of large organic molecules attaching to more than one adsorption site on a metal surface has been reported in the literature.<sup>46-49</sup> The Langmuir adsorption model had erroneously assumed a monolayer adsorption of organic molecules on a metal surface. From the intercepts of the graphs in Figure 11, the value

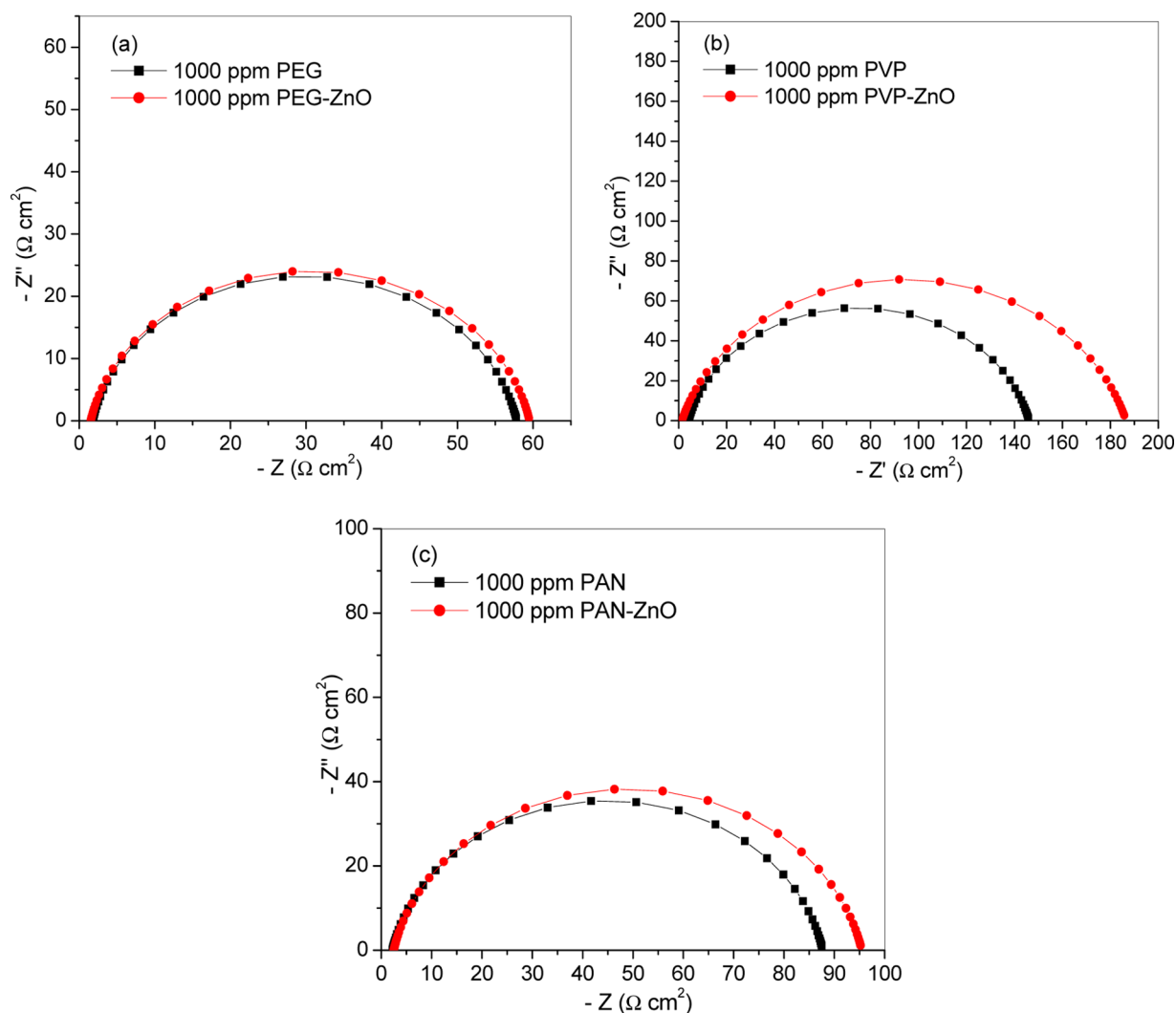


**Figure 10.** Nyquist diagrams for mild steel in 5% HCl with maximum concentrations of 1000 ppm of (a) PEG and ZnO/PEG, (b) PVP and ZnO/PVP, and (c) PAN and ZnO/PAN.

of  $K_{\text{ads}}$  is computed and listed in Table 5. Using the  $K_{\text{ads}}$  value, Gibb's Free energy ( $\Delta G_{\text{ads}}^{\circ}$ ) of the adsorption process also given in Table 5 was calculated thus<sup>50</sup>

$$\Delta G_{\text{ads}}^{\circ} = -RT \ln(1 \times 10^6 K_{\text{ads}}) \quad (7)$$

where  $1 \times 10^6$  represents the concentration of water in the solution expressed in ppm,  $T$  represents the absolute temperature, and  $R$  is the universal gas constant. The  $K_{\text{ads}}$  and  $\Delta G_{\text{ads}}^{\circ}$  values (Table 5) fall into the range of values interpreted in the literature<sup>12,15</sup> for mixed adsorption, i.e., physisorption and chemisorption. The negative sign of the  $\Delta G_{\text{ads}}^{\circ}$  value signifies that the ZnO/polymer nanocomposites adsorb on the metal surface spontaneously and guarantees the stability of the adsorbed layer.

**3.5. Mechanism of Inhibition.** The adsorption of organic inhibitors on the metal surface is accepted to be a substitution adsorption process because water molecules adsorbed on the metal surface are replaced by organic inhibitor molecules.<sup>51</sup> As noted from the experimental results in Tables 2 and 3, the increase in the quantity of the inhibitor improved the corrosion inhibition of the mild steel specimens in 5% HCl. This indicates that more molecules of the studied ZnO/polymer nano-

composites were adsorbed on the surface of the mild steel at higher concentrations, resulting in greater surface coverage.

The order of inhibition performance achieved by the studied ZnO/polymer nanocomposites for mild steel corrosion in 5% HCl at the maximum concentration of 1000 ppm from the EIS result is as follows: ZnO/PVP > ZnO/PAN > ZnO/PEG. The adsorption of the inhibitor molecules would take place through the heteroatoms such as O and N as well as  $\pi$ -bonds.<sup>52–54</sup> The inhibition efficiency is expected to increase in the order N > O.<sup>55</sup> Other factors such as molecular weight, solubility, and structure of the inhibitors would also influence adsorption cum inhibition.<sup>56,57</sup> The molecular structures of PEG, PVP, and PAN indicate that PEG possesses only oxygen atom, PVP possesses nitrogen and oxygen heteroatoms, and PAN contains only nitrogen atom. It has been reported that nitrogen-containing inhibitors tend to perform optimally as corrosion inhibitors in hydrochloric acid.<sup>58,59</sup> Also, chelating rings present in PVP cause an increase in the electron density on the nitrogen heteroatom. This might inform the higher inhibition potential of PVP compared to that of PEG and PAN. PAN acts as a more effective inhibitor of mild steel compared with PEG due to its high molecular weight, the possession of triple bond, and the presence of nitrogen atom. The major setback with PAN is its

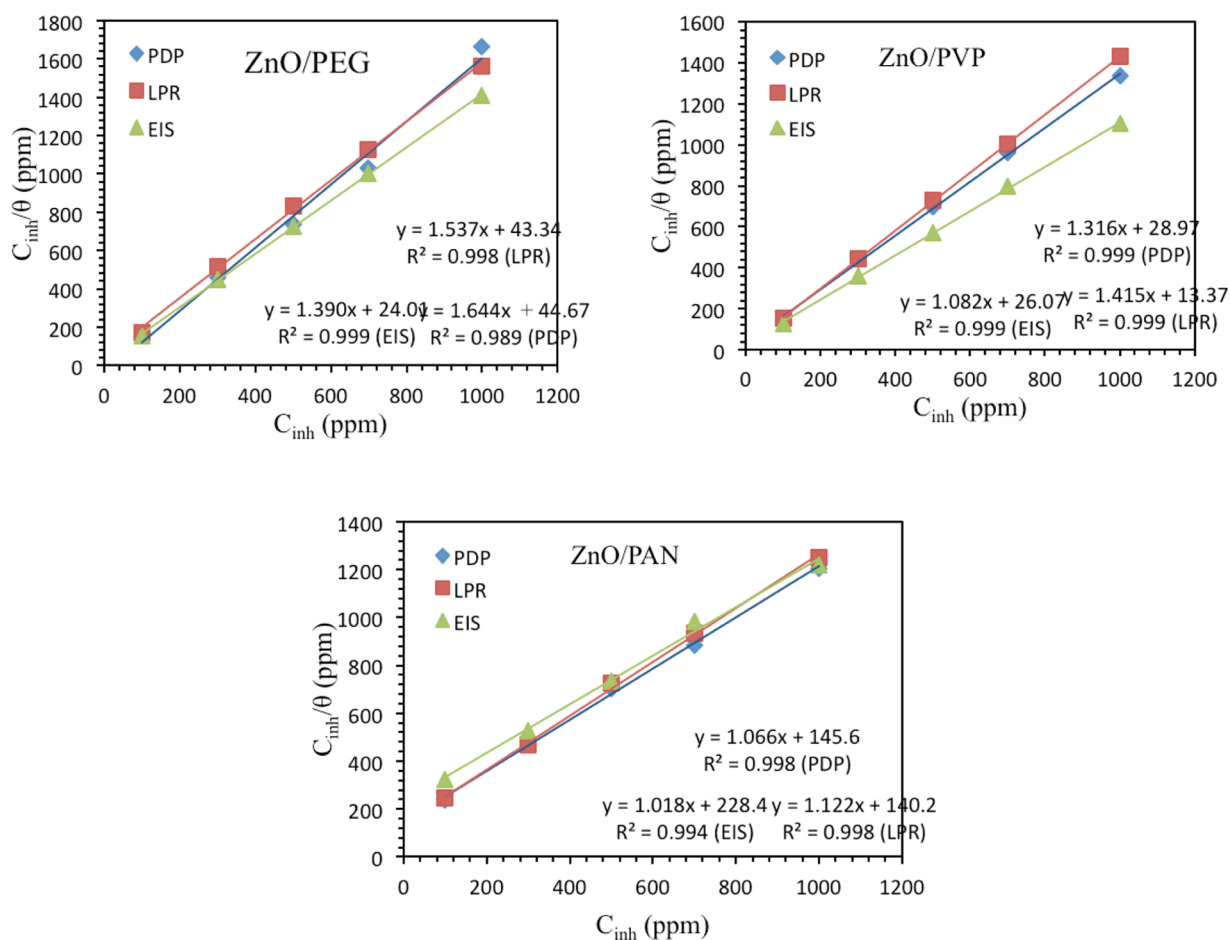


**Figure 11.** Langmuir adsorption graphs for metal dissolution in 5% HCl with various concentrations of ZnO/PEG, ZnO/PVP, and ZnO/PAN, respectively, from different methods.

**Table 5. Values of  $K_{\text{ads}}$  and  $\Delta G^{\circ}_{\text{ads}}$  Obtained from the Langmuir Adsorption Isotherm Graphs for the Studied Inhibitors on Mild Steel in 5% HCl at 303 K**

inhibitor	method	slope	$K_{\text{ads}}$ (ppm/mol)	$-\Delta G^{\circ}_{\text{ads}}$ (kJ mol <sup>-1</sup> )
ZnO/PEG	EIS	1.390	0.0416	26.80
	PDP	1.644	0.0224	25.23
	LPR	1.537	0.0231	25.31
ZnO/PVP	EIS	1.082	0.0384	26.59
	PDP	1.316	0.0345	26.32
	LPR	1.415	0.0748	28.27
ZnO/PAN	EIS	1.018	0.0044	21.12
	PDP	1.066	0.0069	22.26
	LPR	1.122	0.0071	22.35

relative insolubility in the corrosive medium. The incorporation of ZnO nanoparticles into these polymers results in the reinforcement of the properties of the polymers. ZnO nanoparticles may also act as a physical barrier against attacking ions in the corrosive medium.<sup>60</sup> According to Morsi et al.,<sup>60</sup> ZnO nanoparticles can increase their surface area such that the ability of the nanocomposites to be adsorbed on the metal surface increase. They can equally interact with the ions liberated during the corrosion reaction and/or cause an increase in the rate probability for the occurrence. Again, the ZnO nanoparticles can enhance the metal anticorrosion effect due to their ability of catalyzing oxygen reduction on the steel surface and thus increase

the nanocomposite ability to plug some pores and defects on the metal surface.<sup>61</sup>

**3.6. Surface Morphological Studies.** The surface morphology of mild steel coupons immersed for 24 h in 5% HCl in the absence and presence of 1000 ppm of the ZnO/polymer nanocomposites was observed using scanning electron microscopy. The surface micrographs provide information on the extent of surface damage caused by the corrosive ions in each of the corrosive media. Figure 12a shows the micrograph image of the freshly abraded mild steel specimen. The surface is free from cracks and pits but only characterized by grove lines resulting from mechanical abrasion. In Figure 12b, the surface of the mild steel specimen can be seen to be severely damaged with observable cracks and pits after 24 h immersion in uninhibited corrosive solution (5% HCl).

The surface morphologies in Figure 12c–e reveal a drastic reduction in the surface damage occasioned by the adsorption of the nanocomposites. The surfaces are smoother compared to the one in Figure 12b. This is in support of the experimental results that ZnO/PEG, ZnO/PVP, and ZnO/PAN respectively retard the corrosion of mild steel in 5% HCl solution.

## 4. CONCLUSIONS

Three polymers (PEG, PVP, and PAN) and their ZnO nanocomposites have been studied for their anticorrosion potentials for mild steel in 5% HCl solution with the use of different characterization and electrochemical techniques. The

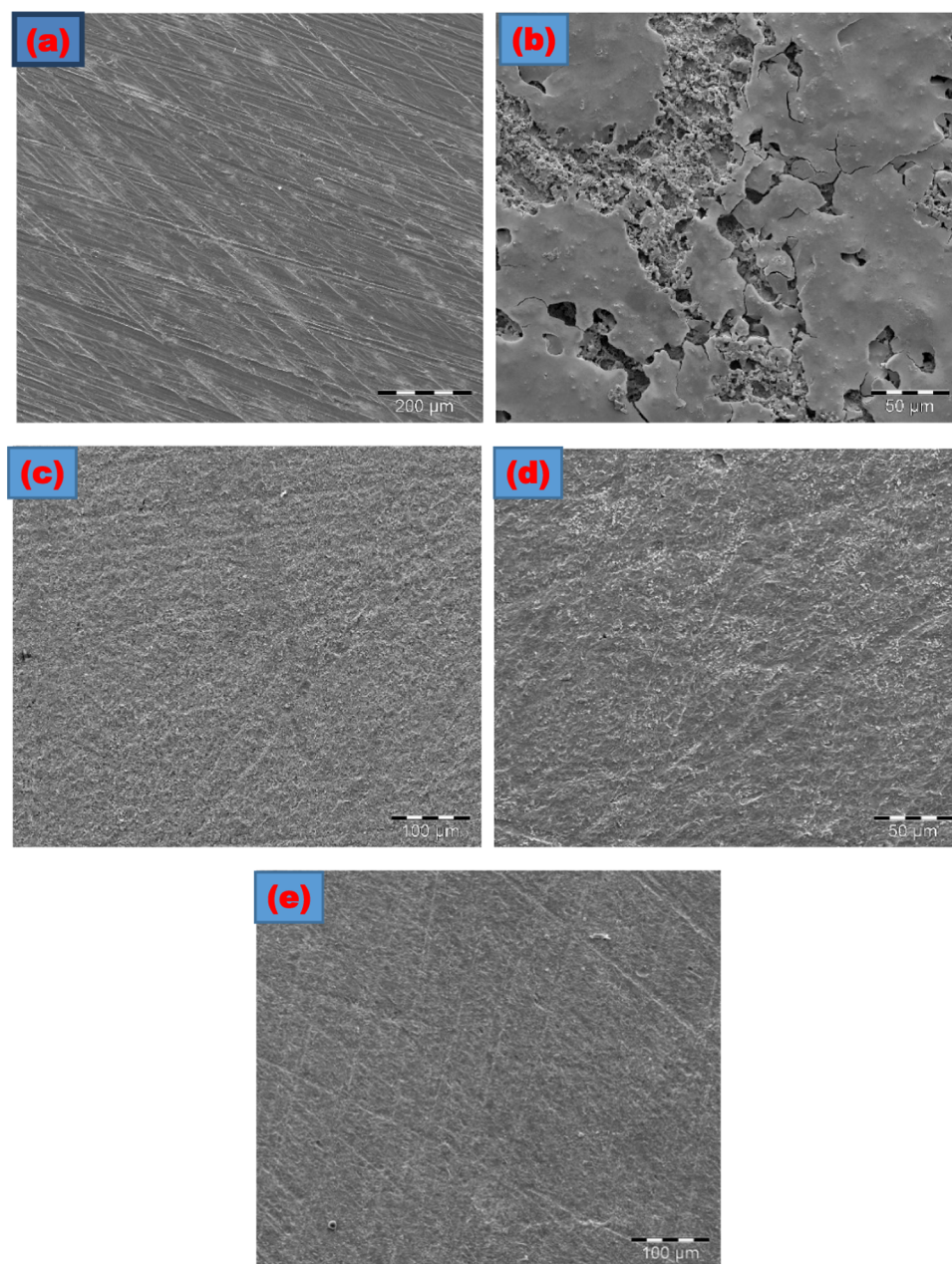


**Figure 12.** SEM micrographs of the mild steel surface (a) freshly abraded, (b) retrieved from 5% HCl, (c) retrieved from 5% HCl + ZnO/PEG, (d) retrieved from 5% HCl + ZnO/PVP, and (e) retrieved from 5% HCl + ZnO/PAN, after 24 h immersion.

following conclusions can be drawn on the basis of the results of the study:

1. Nanocomposites of ZnO/PEG, ZnO/PVP, and ZnO/PAN have been successfully synthesized by the chemical method and characterized using FTIR, UV-vis, TGA, and TEM techniques.
2. TGA results showed that ZnO/polymer nanocomposites are more thermally stable than individual polymer molecules (without the metal oxide).
3. The nanocomposites effectively repressed the dissolution of mild steel in 5% HCl solution, and the anticorrosion performance increased with an increase in the concentration of the inhibitors.
4. Potentiodynamic polarization studies revealed that the inhibitors exhibit a mixed-type effect on mild steel dissolution in 5% HCl solution.
5. The order of efficiency of inhibition is ZnO/PVP > ZnO/PAN > ZnO/PEG.
6. ZnO/polymer nanocomposites adsorb onto the surface of mild steel by both physisorption and chemisorption processes, which can be explained with the Langmuir adsorption isotherm model.
7. SEM images support experimental results that ZnO/PEG, ZnO/PVP, and ZnO/PAN are effective inhibitors for mild steel in 5% HCl solution.

#### ■ AUTHOR INFORMATION

##### Corresponding Author

\*E-mail: [Eno.Ebenso@nwu.ac.za](mailto:Eno.Ebenso@nwu.ac.za). Tel: +27183892050/2051. Fax: +27183892052.

ORCID 

Moses M. Solomon: 0000-0002-3251-8846

Eno E. Ebenso: 0000-0002-0411-9258

## Notes

The authors declare no competing financial interest.

## ACKNOWLEDGMENTS

T.W.Q. acknowledges the National Research Foundation for support toward his postgraduate studies. L.O.O. is grateful to the North-West University for granting him postdoctoral fellowship. E.E.E. thanks the NRF of South Africa for incentive funding for rated researchers.

## REFERENCES

- (1) Durowaye, S. I.; Durowaye, V. O.; Begusa, B. M. Corrosion inhibition of mild steel in acidic medium by methyl red (2,4-dimethylamino-2'-carboxylazobenzene). *Int. J. Eng. Res. Technol.* **2014**, *4*, 469–475.
- (2) Rajeev, P.; Surendranathan, A. O.; Murthy, C. S. Corrosion mitigation of the oil well steels using organic inhibitors—a review. *J. Mater. Environ. Sci.* **2012**, *3*, 856–869.
- (3) Fu, J. J.; Zang, H. S.; Wang, Y.; Li, S. N.; Chen, T.; Liu, X. D. Experimental and theoretical study on the inhibition performances of quinoxaline and its derivatives for the corrosion of mild steel in hydrochloric acid. *Ind. Eng. Chem. Res.* **2012**, *51*, 6377–6386.
- (4) Corrosion inhibitors market analysis by product (organic, inorganic), by application (water-based, oil-based), by end-use (power generation, oil and gas, metal processing, pulp and paper, chemical processing) and segment forecasts to 2024. [www.grandviewresearch.com/industry-analysis/corrosion-inhibitors-market](http://www.grandviewresearch.com/industry-analysis/corrosion-inhibitors-market) (accessed 26 July, 2017).
- (5) Nasibi, M.; Mohammady, M.; Ghasemi, E.; Ashrafi, A.; Zaarei, D.; Rashed, G. Corrosion inhibition of mild steel by Nettle (*Urticadioica* L.) extract: polarization, EIS, AFM, SEM and EDS studies. *J. Adhes. Sci. Technol.* **2013**, *27*, 1873–1885.
- (6) Umoren, S. A.; Ebenso, E. E.; Okafor, P. C.; Ogbobe, O. Water-soluble polymers as corrosion inhibitors. *Pigm. Resin Technol.* **2006**, *35*, 346–352.
- (7) Shanthi, T.; Rajendran, S. Influence of polyacrylamide on corrosion resistance of mild steel simulated concrete pore solution prepared in well water. *IOSR J. Appl. Chem.* **2013**, *5*, 25–29.
- (8) Hefni, H. H.; Azzam, E. M.; Badr, E. A.; Hussein, M.; Tawfik, S. M. Synthesis, characterization and anticorrosion potentials of chitosan-g-PEG assembled on silver nanoparticles. *Int. J. Biol. Macromol.* **2016**, *83*, 297–305.
- (9) Solomon, M. M.; Umoren, S. A. In-situ preparation, characterization and anticorrosion property of polypropylene glycol/silver nanoparticles composite for mild steel corrosion in acid solution. *J. Colloid Interface Sci.* **2016**, *462*, 29–41.
- (10) Solomon, M. M.; Umoren, S. A.; Israel, A. U.; Ebenso, E. E. Polypropylene glycol-silver nanoparticle composites: a novel anti-682 corrosion material for aluminium in acid medium. *J. Mater. Eng. Perform.* **2015**, *24*, 4206–4218.
- (11) Solomon, M. M.; Umoren, S. A.; Abai, E. J. Poly (methacrylic acid)/silver nanoparticles composites: in-situ preparation, characterization and anticorrosion property for mild steel in H<sub>2</sub>SO<sub>4</sub> solution. *J. Mol. Liq.* **2015**, *212*, 340–351.
- (12) Solomon, M. M.; Umoren, S. A. Performance assessment of poly (methacrylic acid)/silver nanoparticles composite as corrosion inhibitor for aluminium in acidic environment. *J. Adhes. Sci. Technol.* **2015**, *29*, 2311–2333.
- (13) Solomon, M. M.; Gerengi, H.; Kaya, T.; Umoren, S. A. Performance evaluation of a chitosan/silver nanoparticles composite on St37 steel corrosion in a 15% HCl Solution. *ACS Sustainable Chem. Eng.* **2017**, *5*, 809–820.
- (14) Solomon, M. M.; Gerengi, H.; Kaya, T.; Umoren, S. A. Enhanced corrosion inhibition effect of chitosan for St37 in 15% H<sub>2</sub>SO<sub>4</sub> environment by silver nanoparticles. *Int. J. Biol. Macromol.* **2017**, *104*, 638–649.
- (15) Solomon, M. M.; Gerengi, H.; Umoren, S. A. Carboxymethyl cellulose/silver nanoparticles composite: synthesis, characterization and application as a benign corrosion inhibitor for St37 steel in 15% H<sub>2</sub>SO<sub>4</sub> medium. *ACS Appl. Mater. Interfaces* **2017**, *9*, 6376–6389.
- (16) Valença, D. P.; Alves, K. G. B.; Melo, C. P. D.; Bouchonneau, N. Study of the efficiency of polypyrrole/ZnO nanocomposites as additives in anticorrosion coatings. *Mater. Res.* **2015**, *18*, 273–278.
- (17) Karthikeyan, P.; Malathy, M.; Rajavel, R. Poly (ophenylenediamine-co-aniline)/ZnO coated on passivated low nickel stainless steel. *J. Sci.: Adv. Mater. Devices* **2017**, *2*, 86–92.
- (18) Alvi, F.; Aslam, N.; Shaikat, S. F. Corrosion inhibition study of zinc oxide-polyanilin nanocomposite for aluminum and steel. *Am. J. Appl. Chem.* **2015**, *3*, 57–64.
- (19) Chouhan, S.; Bajpai, A. K.; Bajpai, J.; Katore, R.; Dhoble, S. J. Mechanical and UV absorption behaviour of zinc oxide nanoparticles: reinforced poly(vinylalcohol-g-acrylonitrile) nanocomposite films. *Polym. Bull.* **2017**, *74*, 4119–4141.
- (20) Luo, Q.; Yang, X.; Zhao, X.; Wang, D.; Yin, R.; Li, X.; An, J. Facile preparation of well-dispersed ZnO/cyclized polyacrylonitrilenanocomposites with highly enhanced visible-light photocatalytic activity. *Appl. Catal., B* **2017**, *204*, 304–315.
- (21) Fayemi, O. E.; Adekunle, A. S.; Ebenso, E. E. Metal oxide nanoparticles/multi-walled carbon nanotube nanocomposite modified electrode for the detection of dopamine: comparative electrochemical study. *J. Biosens. Bioelectron.* **2015**, *6*, 190–203.
- (22) Thirugnanam, T. Effect of polymers (PEG and PVP) on sol-gel synthesis of micro-sized zinc oxide. *J. Nanomater.* **2013**, *2013*, 43–49.
- (23) Rao, N. S.; Rao, M. V. B. Structural and optical investigation of ZnO nanoparticles synthesized from zinc chloride and zinc nitrate. *Am. J. Mater. Sci.* **2015**, *5*, 66–68.
- (24) Matinise, N.; Fuku, X. G.; Kaviyarasu, K.; Mayedwa, N.; Maaza, M. ZnO nanoparticles via *Moringaoleifera* green synthesis: physical properties and mechanism of formation. *Appl. Surf. Sci.* **2017**, *406*, 339–347.
- (25) Shamsuzzaman; Mashrai, A.; Khanam, H.; Aljawfi, R. N. Biological synthesis of ZnO nanoparticles using *C. albicans* and studying their catalytic performance in the synthesis of steroidal pyrazolines. *Arabian J. Chem.* **2017**, *10*, S1530–S1536.
- (26) Barrak, H.; Saied, T.; Chevallier, P.; Laroche, G.; M'nif, A.; Hamzaoui, A. H. Synthesis, characterization, and functionalization of ZnO nanoparticles by N-(trimethoxysilylpropyl) ethylenediaminetriacetic acid (TMSEDTA): Investigation of the interactions between Phloroglucinol and ZnO@ TMSEDTA. *Arabian J. Chem.*, in press, **2016**. [10.1016/j.arabjc.2016.04.019](https://doi.org/10.1016/j.arabjc.2016.04.019).
- (27) Zhang, H.; Xu, L.; Yang, F.; Geng, L. The synthesis of polyacrylonitrile/carbon nanotube microspheres by aqueous deposition polymerization under ultrasonication. *Carbon* **2010**, *48*, 688–695.
- (28) Muşat, V.; Tăbăcaru, A.; Vasile, B. Ş.; Surdu, V. A. Size-dependent photoluminescence of zinc oxide quantum dots through organosilane functionalization. *RSC Adv.* **2014**, *4*, 63128–63136.
- (29) Hussein, M. A.; Abu-Zied, B. M.; Asiri, A. M. Preparation, characterization, and electrical properties of ZSM-5/PEG composite particles. *Polym. Compos.* **2014**, *35*, 1160–1168.
- (30) Mali, S. S.; Kim, H.; Jang, W. Y.; Park, H. S.; Patil, P. S.; Hong, C. K. Novel synthesis and characterization of mesoporous ZnO nanofibers by electrospinning technique. *ACS Sustainable Chem. Eng.* **2013**, *1*, 1207–1213.
- (31) Shao, D.; Gao, D.; Wei, Q.; Tao, L.; Zhu, H.; Ge, M. Deposition of ZnO on polyacrylonitrile fiber by thermal solvent coating. *Fibers Polym.* **2011**, *12*, 214–219.
- (32) Nataraj, S. K.; Kim, B. H.; Yun, J. H.; Lee, D. H.; Aminabhavi, T. M.; Yang, K. S. Electrospun nanocomposite fiber mats of zinc-oxide loaded polyacrylonitrile. *Carbon Lett.* **2008**, *9*, 108–114.
- (33) Umoren, S. A.; Solomon, M. M.; Israel, A. U.; Eduok, U. M.; Jonah, A. E. Comparative study of the corrosion inhibition efficacy of polypropylene glycol and poly (methacrylic acid) for mild steel in acid solution. *J. Dispersion Sci. Technol.* **2015**, *36*, 1721–1735.



- (34) Rivera-Grau, L. M.; Casales, M.; Regla, I.; Ortega-Toledo, D. M.; Ascencio-Gutierrez, J. A.; Porcayo-Calderon, J.; Martinez-Gomez, L. Effect of organic corrosion inhibitors on the corrosion performance of 1018 carbon steel in 3% NaCl solution. *Int. J. Electrochem. Sci.* **2013**, *8*, 2491–2503.
- (35) Olasunkanmi, L. O.; Obot, I. B.; Kabanda, M. M.; Ebenso, E. E. Some quinoxalin-6-yl derivatives as corrosion inhibitors for mild steel in hydrochloric acid: experimental and theoretical studies. *J. Phys. Chem. C.* **2015**, *119*, 16004–16019.
- (36) El-Mahdy, G. A.; Atta, A. M.; Al-Lohedan, H. A.; Tawfik, A. M.; Abdel-Khalek, A. Application of silica/polyacrylamide nanocomposite as anticorrosive layer for steel. *Int. J. Electrochem. Sci.* **2015**, *10*, 151–161.
- (37) Manssour, M.; El Ouadi, Y.; Znini, M.; Costa, J.; Bouyanzer, A.; Desjobert, J. M.; Majidi, L. Adsorption properties and inhibition of mild steel corrosion in HCl solution by the essential oil from fruit of Moroccan *Ammodaucus leucotrichus*. *J. Mater. Environ. Sci.* **2015**, *6*, 631–646.
- (38) Zhang, X.; Zheng, Y.; Wang, X.; Yan, Y.; Wu, W. Corrosion inhibition of N80 steel using novel diquaternary ammonium salts in 15% hydrochloric acid. *Ind. Eng. Chem. Res.* **2014**, *53*, 14199–14207.
- (39) Mashuga, M. E.; Olasunkanmi, L. O.; Ebenso, E. E. Experimental and theoretical investigation of the inhibitory effect of new pyridazine derivatives for the corrosion of mild steel in 1 M HCl. *J. Mol. Struct.* **2017**, *1136*, 127–139.
- (40) Biswas, A.; Pal, S.; Udayabhanu, G. Experimental and theoretical studies of xanthan gum and its graft co-polymer as corrosion inhibitor for mild steel in 15% HCl. *Appl. Surf. Sci.* **2015**, *353*, 173–183.
- (41) Sasikumar, Y.; Adekunle, A. S.; Olasunkanmi, L. O.; Bahadur, I.; Baskar, R.; Kabanda, M. M.; Ebenso, E. E. Experimental, quantum chemical and Monte Carlo simulation studies on the corrosion inhibition of some alkyl imidazolium ionic liquids containing tetrafluoroborate anion on mild steel in acidic medium. *J. Mol. Liq.* **2015**, *211*, 105–118.
- (42) Yadav, D. K.; Quraishi, M. A.; Maiti, B. Inhibition effect of some benzylidenes on mild steel in 1 M HCl: an experimental and theoretical correlation. *Corros. Sci.* **2012**, *55*, 254–266.
- (43) Olasunkanmi, L. O.; Obot, I. B.; Ebenso, E. E. Adsorption and corrosion inhibition properties of N-{n-[1-R-5-(quinoxalin-6-yl)-4, 5-dihydropyrazol-3-yl] phenyl} methanesulfonamides on mild steel in 1 M HCl: experimental and theoretical studies. *RSC Adv.* **2016**, *6*, 86782–86797.
- (44) Umoren, S. A.; Solomon, M. M. Synergistic corrosion inhibition effect of metal cations and mixtures of organic compounds: A Review. *J. Environ. Chem. Eng.* **2017**, *5*, 246–273.
- (45) Alam, R.; Mobin, M.; Aslam, J. Investigation of anti-corrosive properties of poly(aniline-co-2-pyridylamine-co-2,3-xylylidine) and its nanocomposite poly(aniline-co-2-pyridylamine-co-2,3-xylylidine)/ZnO on mild steel in 0.1 M HCl. *Appl. Surf. Sci.* **2016**, *368*, 360–367.
- (46) Mashuga, M. E.; Olasunkanmi, L. O.; Adekunle, A. S.; Yesudass, S.; Kabanda, M. M.; Ebenso, E. E. Adsorption, thermodynamic and quantum chemical studies of 1-hexyl-3-methylimidazolium based ionic liquids as corrosion inhibitors for mild steel in HCl. *Materials* **2015**, *8*, 3607–3632.
- (47) Solomon, M. M.; Umoren, S. A.; Udosoro, I. I.; Udoh, A. P. Inhibitive and adsorption behaviour of carboxymethyl cellulose on mild steel corrosion in sulphuric acid solution. *Corros. Sci.* **2010**, *52*, 1317–1325.
- (48) Migahed, M. A.; Mohamed, H. M.; Al-Sabagh, A. M. Corrosion inhibition of H-11 type carbon steel in 1 M hydrochloric acid solution by N-propyl amino lauryl amide and its ethoxylated derivatives. *Mater. Chem. Phys.* **2003**, *80*, 169–175.
- (49) Abdul Azim, A. A.; Shalaby, L. A.; Abbas, H. Mechanism of the corrosion inhibition of Zn anode in NaOH by gelatine and some inorganic anions. *Corros. Sci.* **1974**, *14*, 21–24.
- (50) Roy, P.; Pal, A.; Sukul, D. Origin of the synergistic effect between polysaccharide and thiourea towards adsorption and corrosion inhibition for mild steel in sulphuric acid. *RSC Adv.* **2014**, *4*, 10607–10613.
- (51) Deyab, M. A.; El-Rehim, S. S. A. Influence of polyethylene glycols on the corrosion inhibition of carbon steel in butyric acid solution: weight loss, EIS and theoretical studies. *Int. J. Electrochem. Sci.* **2013**, *8*, 12613–12627.
- (52) Ebenso, E. E.; Obot, I. B.; Murulana, L. C. Quinoline and its derivatives as effective corrosion inhibitors for mild steel in acidic medium. *Int. J. Electrochem. Sci.* **2010**, *5*, 1574–1586.
- (53) John, S.; Kuruvilla, M.; Joseph, A. Surface morphological and impedance spectroscopic studies on the interaction of polyethylene glycol (PEG) and polyvinyl pyrrolidone (PVP) with mild steel in acid solutions. *Res. Chem. Intermed.* **2013**, *39*, 1169–1182.
- (54) Verma, C.; Ebenso, E. E.; Vishal, Y.; Quraishi, M. A. Dendrimers: a new class of corrosion inhibitors for mild steel in 1 M HCl: Experimental and quantum chemical studies. *J. Mol. Liq.* **2016**, *224*, 1282–1293.
- (55) John, S.; Joseph, A. Electroanalytical and theoretical investigations of the corrosion inhibition behaviour of Bis-1, 2, 4-Triazole Precursors EBATT and BBATT on mild steel in 0.1 N HNO<sub>3</sub>. *Ind. Eng. Chem. Res.* **2012**, *51*, 16633–16642.
- (56) Saadouni, M.; Larouj, M.; Salghi, R.; Lgaz, H.; Jodeh, S.; Zougagh, M.; Souizi, A. Evaluation of corrosion inhibition of mild steel in 1.0 M HCl by sulfathiazole: experimental and theoretical studies. *Pharm. Lett.* **2016**, *8*, 96–107.
- (57) Zarrok, H.; Zarrouk, A.; Salghi, R.; Ramli, Y.; Hammouti, B.; Al-Deyab, S. S.; Oudda, H. Adsorption and inhibition effect of 3-methyl-1-propargylquinoxalin-2 (1H)-one on carbon steel corrosion in hydrochloric acid. *Int. J. Electrochem. Sci.* **2012**, *7*, 8958–8973.
- (58) Verma, C.; Quraishi, M. A.; Korde, R. Corrosion inhibition and adsorption behaviour of 5-(phenylthio)-3H-pyrrole-4-carbonitriles on mild steel surface in 1 M H<sub>2</sub>SO<sub>4</sub>: experimental and computational approach. *Anal. Bioanal. Electrochem.* **2016**, *8*, 1012–1032.
- (59) Zarrouk, A.; Hammouti, B.; Dafali, A.; Bouachrine, M.; Zarrok, H.; Boukhris, S.; Al-Deyab, S. S. A. A theoretical study on the inhibition efficiencies of some quinoxalines as corrosion inhibitors of copper in nitric acid. *J. Saudi Chem. Soc.* **2014**, *18*, 450–455.
- (60) Morsi, R. E.; Labena, A.; Khamis, E. A. Core/shell (ZnO/polyacrylamide) nanocomposite: in-situ emulsion polymerization, corrosion inhibition, anti-microbial and anti-biofilm characteristics. *J. Taiwan Inst. Chem. Eng.* **2016**, *63*, 512–522.
- (61) Ganash, A. Anticorrosive properties of poly (o-phenylenediamine)/ZnO nanocomposites coated stainless steel. *J. Nanomater.* **2014**, *2014*, 1–8.